Targeting STUB1–tissue factor axis normalizes hyperthrombotic uremic phenotype without increasing bleeding risk

Citation: Shashar, Moshe et al. "Targeting STUB1–tissue Factor Axis Normalizes Hyperthrombotic Uremic Phenotype Without Increasing Bleeding Risk." Science Translational Medicine 9, 417 (November 2017): eaam8475 © 2017 The Authors

As Published: http://dx.doi.org/10.1126/scitranslmed.aam8475

Publisher: American Association for the Advancement of Science (AAAS)

Persistent URL: http://hdl.handle.net/1721.1/114286

Version: Author's final manuscript: final author's manuscript post peer review, without publisher's formatting or copy editing

Targeting STUB1-tissue factor axis normalizes the hyperthrombotic uremic phenotype without increasing the bleeding risk

Moshe Shashar[1*], Mostafa E. Belghasem[2*], Shinobu Matsuura[3], Joshua Walker[1], Sean Richards[1], Faisal Alousi[1], Keshab Rijal[1], Vijaya B. Kolachalama[3], Mercedes Balcells[4,5], Minami Odagi[6], Kazuo Nagasawa[6], Joel M. Henderson[2], Amitabh Gautam[7], Richard Rushmore[9], Jean Francis[1], Daniel Kirchhofer[10], Kumaran Kolandaivelu[4,8], David H. Sherr[11], Elazer R. Edelman[4,8], Katya Ravid[3], Vipul C. Chitalia[1,2,3]

* = Equal contribution

Author affiliations:
[1] Renal Section, Department of Medicine, Boston University School of Medicine, Boston, MA, USA
[2] Department of Pathology and Laboratory Medicine, Boston University School of Medicine, Boston, MA, USA
[3] Department of Medicine and Whitaker Cardiovascular Institute, Boston University School of Medicine, Boston, MA, USA
[4]Institute of Medical Engineering and Science, Massachusetts Institute of Technology, Cambridge, MA, USA
[5] Biological Engineering Department, Institut Químic de Sarrià, Ramon Llull Univ, Barcelona, Spain
[6] Department of Agriculture and Sciences, Tokyo University, Japan
[7] Department of Surgery, Boston University School of Medicine, Boston, MA, USA
[8] Cardiovascular Division, Brigham and Women's Hospital, Harvard Medical School, Boston, MA, USA
[9] Department of Anatomy and Neurobiology, Boston University School of Medicine, Boston, MA, USA
[10] Department of Early Discovery and Biochemistry, Genentech Inc., South San Francisco, CA 94080, USA
[11] Department of Environmental Health, School of Public Health, Boston University School of Medicine, Boston, MA, USA

*__Corresponding author__:
Vipul Chitalia, M.D., Ph.D.
Department of Medicine
Boston University Medical Center
Evans Biomedical Research Center, X-530
Boston, MA 02118, USA
(P) 617-638-7330
(F) 617-638-7326
email: vichital@bu.edu

Conflict of interest: The authors do not report any conflict of interest.

Abstract:

Chronic kidney disease (CKD/uremia) remains vexing as it is associated with increased atherothrombosis but also increased complications with standard antithrombotic/antiplatelet therapies. Though associations of uremic solutes (e.g. indolic solutes) and vascular wall proteins (such as tissue factor - TF and Aryl Hydrocarbon Receptor - AHR)) are being defined, the specific mechanisms that drive the thrombotic and bleeding risks have not been fully understood nor means by which they might be therapeutically manipulated. We now present an indolic solute-specific animal model, which focuses on solute-protein interactions and show that indolic solutes mediate the hyperthrombotic phenotype across all CKD stages in an AHR- and TF-dependent manner. We demonstrate further that AHR regulates TF through Carboxy terminus Hsc70 interacting protein (CHIP/STUB1). As an ubiquitin ligase, STUB1 interacts dynamically with and degrades TF through ubiquitination in a uremia-dependent manner. TF regulation by STUB1 is substantiated in humans by an inverse relationship of STUB1 and TF expression and reduced STUB1-TF interaction in uremic vessels. STUB1's enhancement using a novel preclinical compound, 2-(4-hydroxy-3-methoxyphenyl)-benzothiazole inhibits post-interventional thrombosis. STUB1 perturbations reverted the uremic hyperthrombotic phenotype to non-CKD range in two discrete animal models of uremia without prolonging the bleeding time. This finding is in stark contrast to Heparin, the standard-of-care antithrombotic in CKD patients. While identifying STUB1 as a TF regulator and by targeting CKD-specific mediators, we expand the understanding of the interconnected relationships that drive the fragile thrombotic state in CKD. Moreover, our work also establishes a new means of minimizing the uremic hyperthrombotic phenotype without altering the hemostatic balance, a long-sought-after combination in CKD patients.

One line summary

Profoundly thrombogenic *milieu* of CKD imposes a unique risk that is not targeted by contemporary antithrombotics, resulting in their dismal efficiency and increased bleeding risk. This paper uncovers a novel mediator of uremic hyperthrombogenicity and demonstrates that targeting this central node of uremic thrombosis axis normalizes the CKD-associated thrombosis risk without altering hemostasis. Combining such a strategy with the contemporary antithrombotic/antiplatelet therapy will improve their efficacy and safety profile in CKD patients.

Introduction:

Chronic kidney disease (CKD/uremia) imposes a strong and independent risk for both venous and arterial thrombosis in addition to conventional risk factors (*1-3*). CKD-associated thrombotic propensities introduce variability, which is not accounted for in the global thrombosis risk assessment nor targeted by the contemporary antithrombotic/antiplatelet therapies. This variability contributes to their suboptimal efficacy in several clinical post-injury arterial thrombosis models such as angioplasty, stenting or vascular surgeries in CKD patients *(2, 4-6)*.

Of the different components of thrombosis, vessel wall factors are critical triggers for the post-vascular injury thrombosis, where denuded endothelium and exposed vascular smooth muscle cells (vSMCs) create a highly reactive vascular bed. Tissue factor (TF), a potent procoagulant protein and the driver of post-injury thrombosis model, is 2-3-fold higher in vSMCs in uremic *milieu* and enhances thrombosis *(7-9)*. Retention of a unique set of metabolites characterizes the state of uremia, of which indolic solutes (indoxyl sulfate- IS) are particularly vasculotoxic (*10*). They enhance the TF expression by activating Aryl hydrocarbon pathway (AHR) and AHR antagonists destabilize and downregulate TF in the uremic *milieu* (*11*). While IS and AHR are emerging regulators of TF, their contribution to the thrombotic uremic *milieu* and the mechanism in CKD warrant further elucidation, as their better understanding will help design the approaches to minimize CKD-specific thrombosis risk.

It is also imperative to weigh the antithrombotic benefit of such an approach to bleeding risk particularly in CKD patients, as uremia is a state of bleeding diathesis (*12*). This risk is further exacerbated by current antithrombotics (*13*), which target the hemostatic defenses in blood. Even the newer antithrombotics that are deemed safer, though not tested specifically in uremic *milieu*, may function sub-optimally in CKD, as none target CKD-specific risk factors (*14*) and may paradoxically enhance thrombosis due to altered baseline platelet reactivity in CKD (*15, 16*). The strategies that lower CKD-associated thrombotic risk will create a *milieu* conducive

to current antithrombotics/antiplatelet agents and are less likely to alter the hemostatic balance given their direct target of disease mediators. While demonstrating IS as an AHR-dependent mediator of the hyperthrombotic uremic *milieu* all across the CKD spectrum, we show that AHR regulates TF through the Carboxy terminus Hsc70 interacting protein (STUB1), a U-box ubiquitin ligase. We also demonstrate that the perturbation of STUB1 reverts the CKD-associated thrombosis risk to non-uremic range without altering the hemostasis. Integration of this strategy will improve the antithrombotic management of CKD patients and allow individualization of care.

Results:

IS mediates a hyperthrombotic uremic phenotype in an AHR-and TF-dependent manner across the spectrum of CKD

To examine the mediators of the hyperthrombotic uremic *milieu in vivo*, different animal models of CKD were considered (*17*). The renal damage inflicted in all of these CKD models results in retention of a whole host of uremic solutes precluding specific probing of a uremic solute. Furthermore, contrary to human CKD, 5/6-nephrectomy model of CKD had failed to show enhanced thrombosis (*18*). Therefore, we set out to create a solute-specific animal model that faithfully recapitulates the hyperthrombotic uremic phenotype. As IS increases TF (*7, 11, 19*), we hypothesized that IS will enhance thrombosis. Towards that end, we first developed an animal protocol to increase the blood levels of IS similar to patients with advanced CKD (CKD stage 5/end stage renal disease, ESRD) by administering IS and inhibiting its excretion through the organic anion transporter (OAT) channel using Probenecid (*20*). Of the different tested protocols of IS and Probenecid administered through oral and intra-peritoneal routes, a combination of IS 4mg/ml in water along with Probenecid 150 mg/kg intra-peritoneal given twice a day resulted in elevation of IS levels beyond the levels of ESRD patients and was selected for further experiments (**Fig. 1A and fig. S1A**). While Probenecid employed in this model inhibited renal excretion of IS, given the ubiquitous expression of OAT channels (*21*), Probenecid may also inhibit OAT channels in vascular smooth muscle cells (vSMCs) to reduce the entry of IS into the cells of vessel wall. Therefore, we examined AHR activation in the vessels of mice that received IS plus Probenecid, using an AHR decay assay (**fig. S1B and S1C**). The assay is based on a fundamental observation that AHR activation with an agnostic ligand such as IS eventually results in the degradation of AHR protein (*11*). Thus, AHR protein levels are likely to be lower in the vessels of animals exposed to IS + Probenecid, if intracellular concentration of IS rises in the presence of Probenecid. Indeed, the aortas of IS + Probenecid mice harvested at

different time points showed a significant and persistent reduction in AHR protein levels throughout the duration of exposure, as compared to Probenecid controls (**fig. S1B and S1C**). Also, a striking increase in TF levels was observed in their aortas (**fig. S1D**). Taken together, these data support an increase in IS levels in the vessel wall as sufficient to activate AHR-TF signaling in mice exposed to IS + Probenecid.

After confirming the activation of AHR-TF axis in the vessel walls of these animals, their thrombogenicity was examined by inflicting arterial injury using $FeCL_3$ on the carotid artery, a well-established post-injury thrombosis model (*22*). The time to reduction in blood flow to baseline (Time to Occlusion, TtO) detected in real-time with an ultrasound probe served as a primary end point (**Fig. 1B and fig. S1E)**, and was validated by an occlusive thrombus at the site of injury (**Fig. 1C**). From a range of $FeCL_3$ concentrations tested, 10% $FeCL_3$ was chosen for its ability to consistently induce thrombosis in the uremic *milieu* (**fig. S1F**).

Under these optimized conditions, compared to Probenecid group, IS significantly reduced TtO (**Fig. 1B and 1D**), which was reversed effectively with AHR antagonist, CH223191 (*11*) or prior infusion of a pre-validated anti-mouse anti-TF neutralizing antibody (*23*) (**Fig. 1E**). To further validate the thrombogenicity of IS, thrombosis was induced by photoactivation of Rose Bengal dye, which produces singlet oxygen to damage endothelial cell membranes (*24-26*). Consistent with the $FeCL_3$ model, IS-treated animals showed a significant reduction in TtO in the photochemical injury model (**Fig. 1F**). While these two models examined the prothrombotic properties of IS at levels corresponding to advanced CKD, we next probed its role in early stages of CKD, as patients with mild CKD are also predisposed to enhanced thrombosis (*11, 27, 28*). IS levels corresponding to the different stages of CKD were achieved in the blood of animals by titrating the IS concentration in water. Resultant blood levels of IS were determined and correlated to the TtO. The data showed a significantly inverse correlation between TtO and IS concentrations corresponding to all CKD stages (**Fig. 1G**). Overall, the

above results support IS as an AHR- and TF-dependent mediator of the hyperthrombotic uremic *milieu* across a CKD spectrum.

AHR regulates TF through STUB1, an ubiquitin ligase for TF

As the above data implicated IS as a strong contributor to hyperthrombotic uremic phenotype, we further probed the mechanism of IS-induced changes in AHR/TF towards promoting thrombogenicity. Here we find that the Carboxy terminus Hsc70 interacting protein (STUB1/CHIP), an ubiquitin ligase and an AHR interactor, mediated the effect of IS/AHR on TF (*29*). *STUB1* silencing in primary human aortic vSMCs and human umbilical vein endothelial cells (thrombosis-relevant cell types) showed significantly increased TF levels (**Fig. 2A and fig. S2A**) and TF activity in both uremic and non-uremic *milieu* (**Fig. 2B**). In line with STUB1's ubiquitin ligase function (*29-31*), *STUB1*-silenced vSMCs showed a significantly prolonged TF half-life under the uremic condition from 3.25 hours to more than 8 hours (**Fig. 2C-2D**) and reduced ubiquitination (**fig. S2B**). CB7993113**,** a competitive AHR antagonist (*11*), reduced TF expression by 80% (from 1.0 to 0.21), while it was only reduced by 30% (from 2.7 to 1.98) with a concomitant *STUB1* silencing (**Fig. 2E**). *STUB1* silencing also abrogated CB7993113-mediated TF ubiquitination in the uremic *milieu* (**Fig. 2F**). Consistent with the above results, mesenchymal embryonic fibroblasts (MEF) from STUB1 KO animals (*30*) showed a significant increase in TF protein levels, and activity, and reduced TF ubiquitination (**fig. S2C-S2E**). Ubiquitin ligase-dependent STUB1 regulation of TF was further demonstrated using an ubiquitin ligase-deficient H260Q STUB1 mutant. Compared to wild-type (WT) STUB1, the H260Q mutant showed little effect on TF ubiquitination (**fig. S2F**). The above results support STUB1 as a mediator of TF ubiquitination, and that AHR antagonist mediates TF regulation through STUB1.

Dynamic uremia-dependent STUB1-TF interaction

Ubiquitination is a nonlinear process consisting of complex interdigitated set of regulated steps, which include ubiquitin activation, conjugation and transfer of the ubiquitin moiety to the target molecule. This process requires a precise and dynamic interaction between a ligase and its putative target. Reciprocal immunoprecipitation (IP) assays in vSMCs demonstrated that anti-TF antibodies co-IPed STUB1, and vice versa (**fig. S3A**). An *in vitro* binding assay demonstrated a direct binding of recombinant STUB1 to purified human TF protein (**Fig. 3A**). Immunofluorescence studies showed co-localization of STUB1 and TF predominantly in the cytosol of vSMCs in normal human artery and cultured vSMCs with Pearson's correlation coefficient of 0.50 and 0.82, respectively (*32*) (**fig. S3B-S3F).** While these data indicated a constitutive interaction between STUB1 and TF, their STUB1-TF interaction was also found to be dynamic and dependent on the uremic status. STUB1-TF interaction reduced substantially with IS (**Fig. 3b**), and increased within 20 minutes of AHR antagonist treatment. This rapidity of increased STUB1-TF interaction induced by AHR antagonist is consistent with the previously observed restoration of TF ubiquitination and shortened TF half-life with AHR antagonist (*11*). Taken together, the above data suggest that uremia reduces STUB1-TF interaction to stabilize TF, and AHR antagonists rapidly restore this interaction.

Furthermore, the site of interaction of STUB1 and TF corroborated the above binding pattern. As STUB1 is known to be a cytosolic protein and TF has a cytosolic C-terminus (**fig. S3C**), STUB1 is likely to target the C-terminus tail of TF. Domain mapping was performed by comparing the wild-type TF (TF-WT) with a TF truncation lacking its C-terminus (TFdelC). STUB1 interacted with TF-WT and downregulated it by 70% (time 0, **Fig. 3C-3F**) and significantly shortened its half-life and increased its ubiquitination. STUB1 had no effect on TFdelC (**Fig. 3C-3F and fig. S3D-S3E**), indicating that STUB1 targets the C-terminus tail of TF for ubiquitination and degradation.

Uremia dependent STUB1-TF relationship in human tissue

Dynamic interaction with and regulation of TF by STUB1 were further substantiated in human vascular tissue using immunofluorescence studies of explanted arteriovenous fistulae (AVF), which is a unique vascular conduit required in patients with advanced CKD, that is frequently prone to thrombosis (*33*) (**table S1**). We posited an inverse relationship between STUB1 and TF, as STUB1 downregulates TF. Our initial examination did reveal opposite expression levels between TF and STUB1 within vSMCs of AVF (**Fig. 3G**). However, the precise demonstration of a relationship between proteins requires their quantification, which is challenging in heterogeneous human tissues using conventional methods (*34*). Therefore, we developed an object-level intensity estimation algorithm to quantify TF and STUB1 expressions. The results confirmed a strong inverse correlation between TF and STUB1 expression in the vSMCs in the walls of AVF explants (**Fig. 3H-3I**). We further posited that reduced STUB1-TF interaction in vSMCs induced by IS (**Fig. 3B**) is likely to reduce STUB1-TF co-localization in the vessel wall. To this end, we compared the STUB1-TF co-localization in human AVF (uremic vessel) and vessels from non-CKD patients (non-uremic control) using a customized co-localization algorithm with pixel-level analysis. The results showed a significant (close to 50%) reduction in the co-localization of STUB1-TF in uremic compared to non-uremic human vessels (**Fig. 3J-3K)**. Taken together, these results indicate STUB1's direct and dynamic interaction with and regulation of TF.

STUB1 modulation regulates post-interventional thrombosis

TF from exposed vascular smooth muscle cells (vSMCs) is a critical trigger of post-injury thrombosis, especially in the uremic *milieu (7-9).* We examined the effect of STUB1 on thrombosis, using the flow-loop system (*35*), a validated model of post-interventional thrombosis (**Fig. 4A-4B**). It specifically examines the blood and vessel-wall factor interactions under humanized rheological conditions, and have recapitulated thrombosis in the uremic *milieu* (*7*).

The flow-loops with STUB1 KO MEFs showed a higher clot formation (**Fig. 4C**) and a significantly higher clot burden (increased hemoglobin and lactic dehydrogenase) (**Fig. 4D**). Next, the effect of STUB1 upregulation on thrombosis was examined using 2-(4-hydroxy-3-methoxyphenyl)-benzothiazole (YL-109), a preclinical anti-cancer STUB1 enhancer compound that increases the protein levels of STUB1 by inducing its transcription (**Fig. 4E**) (*36*). YL-109 significantly inhibited IS-induced thrombosis in flow-loops (**Fig. 4F**). In same line, we observed a dose-dependent reduction in TF levels and TF activity along with doubling of STUB1 levels in vSMCs (**Fig. 4G-4H and fig. S4**). Since YL-109 increases STUB1 protein levels, it is likely to enhance TF ubiquitination, which was examined using co-expression of ubiquitin (Ub) and TF in the presence of uremic serum. YL-109 treatment increased the higher molecular weight polyubiquitinated TF in vSMCs (**Fig. 4I**). Taken together, these data suggest that increase in STUB1 levels in vSMCs enhances TF ubiquitination and degradation and inhibits hyperthrombotic uremic *milieu*.

IS-AHR-STUB1 axis modulation reverses the hyperthrombotic uremic phenotype to non-CKD range without altering the hemostatic barrier

We next examined if augmented STUB1 suppressed the hyperthrombotic uremic *milieu in vivo* using the indolic-solute specific animal model (**Fig. 1**). The effects were compared to Heparin, which is a standard-of-care antithrombotic in CKD patients (**Fig. 5A**). Compared to the IS group, YL-109 significantly prolonged the TtO (**Fig. 5B-5C**) with no significant differences in IS levels in between these groups (**fig. S5A**). As STUB1-TF is a CKD-specific thrombotic pathway, we posited its targeting by YL-109 is likely to revert the thrombogenicity to the non-CKD range. Therefore, we compared the effect of YL-109 to the Probenecid (non-CKD) controls. The results showed no significant difference in TtO with IS + YL-109 compared to Probenecid controls. On the other hand, Heparin at a dose considered therapeutic in humans (*37*) significantly prolonged TtO compared to both IS and Probenecid controls (**Fig. 5C**). YL-

109-treated animals showed a significant increase in STUB1 and decrease in TF levels in their aortas (**Fig. 5D and fig. S5B**). To further probe a quantitative link between changes in TF levels and thrombogenicity *in vivo*, we correlated the reduction of TF levels in the aortic lysates of individual mice exposed to IS + YL-109 to their prolongation of TtO. We hypothesized that both these parameters will inversely correlate should reduction in TF levels in the vessel wall reduce the thrombogenicity in uremic *milieu.* Indeed, a significant negative correlation (Spearman rho = -0.833 and p = 0.02) between the reduction in TF levels within the vessel wall and prolongation of TtO was observed in mice treated with YL-109 (**Fig. 5E**). Taken together, these data strongly suggest that reduction in TF by STUB1 regressed the hyperthrombotic uremic phenotype to the non-CKD range.

Since the solute-specific animal model partially recapitulates the uremic phenotype, these results warranted further validation in an established model of CKD. Among different animal models of CKD, the proteinuric CKD model and hypertensive model are likely to confound the thrombosis assay due to loss of anti- and prothrombotic factors in the urine (*38*) and increased endothelin level, respectively, in these models (*39*). Therefore, we used the Adenine-induced renal injury model, a well-established model of uremia induced by extensive tubulointerstitial fibrosis (*40, 41*) (**fig. S5C**). The animals showed significant increases in blood urea nitrogen (BUN) and IS levels corresponding to advanced CKD patients within two weeks of 0.25% Adenine diet (**Fig. 5F and fig. S5D**). A significant reduction in TtO was observed in the Adenine-induced CKD animals compared to animals on a regular chow diet, further supporting CKD as a hyperthrombotic environment. In the Adenine-treated group, the TtO was significantly prolonged upon treatment with CH223191 (p = 0.004), or YL-109 (p = 0.050), compared to the vehicle-treated (control) group (**Fig. 5G**). Furthermore, similar to the indolic solute-specific model (**Fig. 5C**), no significant differences in TtO were noted in the CH223191 (p = 0.374) and YL-109-treated (p = 0.983) groups when compared to the animals on a regular chow diet (non-

CKD animals). All these data obtained from two independent models strongly argue for CKD as a hyperthrombotic *milieu*, and that uremia-induced thrombogenicity is normalized to a non-CKD range with the modulation of AHR-STUB1 axis.

The antithrombotic effects of the above agents were weighed against the bleeding risk using the standard tail vein transection model (*22*). As STUB1 modulation normalized the thrombotic risk to non-CKD range, we compared YL-109-mediated alteration in bleeding time to Probenecid (non-CKD) controls. The data showed a non-significant reduction in bleeding time with IS compared to Probenecid controls (**Fig. 5H**). Interestingly, compared to the Probenecid controls, no significant increase in the bleeding time was noted with YL-109 (**Fig. 5H**) and fell within the two SD range of the non-CKD controls' bleeding time (clear area, **Fig. 5I**). In contrast, Heparin significantly prolonged the bleeding time beyond 2SD of Probenecid controls (shaded area, **Fig. 5I**). Overall these data indicate that, unlike Heparin, STUB1 modulation reverted the IS-mediated hyperthrombotic phenotype to the non-uremic range without enhancing the bleeding risk.

Discussion:

CKD patients are prone to thrombosis and are specifically sensitive to what are relatively CKD-nonspecific antithrombotic and antiplatelet agents (*12, 13, 42*). The CKD patients are at 4 fold-increased risk of bleeding, which is further augmented by 50% with every 30 ml/min decrease in creatinine clearance (*43-45*). To some this implies that a CKD patient represents an extreme case of classic vascular disease and to others that the CKD *milieu* is distinct and unique. Our data support the latter and implicate IS in particular as a mediator of the hyperthrombotic uremic state by modulating STUB1-TF interaction. Here, we show that reduced STUB1-TF interaction in vSMCs in uremia stabilizes TF and augments thrombosis upon exposure to vascular injury. Conversely, restoration of STUB1-TF interaction by suppression of uremic effect by AHR antagonist or STUB1 inducer augments TF ubiquitination and degradation and inhibits thrombosis. While discerning the antithrombotic mechanism of AHR antagonist and adding to the sophistication of the complex vascular biology of CKD, these data highlight the role of dynamic protein-protein interaction influenced by the uremic state, which we further substantiate in human vessels. We also demonstrate the prominent role of STUB1-TF axis in mediating CKD-specific thrombotic risk, which reverses to non-CKD range upon pharmacological targeting.

While several possibilities can contribute to the dynamic interaction of STUB1 and TF, rapid modulation of this interaction with AHR status argues for the role of AHR and post-translational modifications (PTM) in this process. As STUB1, AHR (*29*) and TF bind to each other (*11*), it is likely that they form a multiprotein complex, which may undergo stoichiometric or conformational changes upon AHR activation (IS treatment) or AHR suppression (AHR antagonist treatment) altering the interactions between the components (**Fig. 3A-3B**) (*29*). The kinetics of STUB1-TF interaction) support PTMs in either or both the partners. Similar PTMs

have been reported to modulate the interaction of STUB1 with other targets (*46, 47*). This rapid STUB1-TF interaction is followed by ubiquitination and proteasomal degradation of TF such that TF protein reaches its half-life within 40 minutes in vSMCs (*11*). The involvement of ubiquitination in regulating TF imparts specificity and efficiency to TF biology. Such a system is built for amplification, as the target (TF) and the ubiquitin ligase (STUB1), and the modifying protein (ubiquitin) are all governed by complex auto- and para-regulatory loops (*48*). It is such a system that can regulate the biology of a central stimulus like TF released and/or exposed on vSMCs early after vascular injury, and especially within the context of the complex uremic *milieu* (*7, 11, 19*). Such biochemistry also explain why modest changes in any of the involved elements induce large, nonlinear effects on outcomes, and a strong *in vivo* correlation between the reduction in thrombogenicity and changes in TF within the vessel wall in response to pharmacological manipulation of STUB1 (**Fig. 5E**).

Even minor changes in TF levels are expected to have a substantial effect on thrombosis, as vessel wall TF activation is only a primary trigger, followed by a multitude of non-linear and interrelated events, such as an extrinsic coagulation cascade and platelet aggregation (*49*), all of which profoundly amplify the primary trigger of TF activation onto robust thrombus formation. Thus, perturbation of TF through AHR-STUB1 axis represents an effective therapeutic strategy in CKD patients, as none of the current antithrombotics or the investigational agents such as Factor XII and XI inhibitors target CKD-specific thrombosis (*14, 15*). Their suboptimum efficacy is likely to be exacerbated due to poor thrombus control from persistent nidus of exposed vSMCs secondary to compromised re-endothelialization of vascular wound under uremic *milieu* (*50*). Compounding poor efficacy profile is their enhanced bleeding risk due to altered pharmacokinetics in CKD and perturbation of critical hemostatic defense (*12, 13, 42, 51*).

Two complementary *in vivo* thrombosis models employed here, involving damaged endothelium, established the relevance of our in vitro studies. The added value of an animal model that specifically involves a uremic solute in the context of vascular injury allows us to directly address individualized CKD-associated risk assessment, and can also drive precision in antithrombotic management. While this novel animal model is a valuable tool for mechanistic probing, and is potentially useful in preclinical drug development, especially with its validation in an established CKD model (**Fig. 5F and 5G**), it does not emulate the human arterial rheological patterns nor the flow characteristics that are critical in post-interventional thrombosis (*52*). The flow loop system used herein (*35*) is a model of post-interventional thrombosis using a humanized system of human cells and human blood simulating human coronary flow patterns. The prediction of thrombosis in the flow loop system has been validated in prospective human clinical trials (*35, 53, 54*). Clot formation is defined by three discrete components, which provide a different view of net extent of thrombosis. For example, Hb and LDH measurements represent red cell content and active remodeling of the clot, respectively, and visual inspection assesses overall clot burden. The results from the flow loops tracked well with the probed genetic loss-of-function of STUB1 (**Fig. 2, 4C and 4D**), or with pharmacological upregulation of STUB1 (**Fig. 4E, 4F and 5A-5D**). Interrogating the AHR-TF-STUB1-TF axis using orthogonal model systems has strengthened the translational significance of this axis.

That we now add two discrete mechanisms of TF downregulation in uremic *milieu* via increasing STUB1 levels (**Fig. 4H and 5D**) and enhanced STUB1-TF interaction (**Fig. 3B**) supports the development of direct STUB1 activators and selective AHR modulators as antithrombotics (*55*). Since the effects of these agents are likely to be influenced by the state of

AHR signaling, an accompanying biomarker based on levels of uremic solutes (*11*) will further refine the risk-benefit profile for antithrombotics in the CKD patients. Moreover, our data suggest that therapy with agents that target disease-specific mechanisms to normalize the uremic hyperthrombotic *milieu* along with the current antiplatelet/antithrombotic might well enhance therapeutic efficacy and safety. Some of the approaches in this study might also have broad applicability. For example, the image processing algorithms can extract rich quantitative data regarding the spatiotemporal expression of proteins and uncover potential relationships in heterogeneous human tissues (*34*). In addition to avoiding confounders such as hypertension in other CKD models (*17*), this novel animal model allows titration of a specific uremic solute to examine its effect at different stages of CKD (**Fig. 1E**).

Thrombosis is a dynamic process orchestrated by several different cell types and mediators, and almost all of these components are altered in CKD (*56*). Though vessel wall factors trigger thrombosis in the post-vascular injury model, contributions of other components such as platelets, microparticles and white blood cells, etc., are also important for thrombosis. This is especially the case given recently reported effects of IS on platelet hyper reactivity and thrombosis (*57*). While the current report demonstrates the role of IS-AHR-STUB1 in TF regulation, it remains to be determined if this axis regulates other thrombotic mediators in uremic or normal states.

Several dynamic events influence thrombosis and hemostasis processes and their precise quantification are required to determine the global thrombosis risk and allow individualization of therapy. CKD-specific thrombosis risk assessment can be performed using uremic solute load in blood, an approach highly desirable given the diabolic nature of uremia (*3, 11, 12*). Accompanying such a risk marker is a means of normalizing CKD-specific thrombosis

risk to non-CKD level, which is likely to improve the antithrombotic management of CKD patients. Our study focused on post-interventional thrombosis in CKD, as these patients carry high cardiovascular disease burden requiring complex vascular procedures and also are at risk of thrombosis of dialysis access, a lifeline of CKD patients. This novel axis needs further probing in other models of thrombosis.

Methods:

Please refer to Supplemental Material for a detailed account of all other methods used.

Human subjects and serum collection: Pooled uremic sera (patients of ESRD on hemodialysis) and age, gender and ethnic background matched control sera are described previously(*7*). Briefly, the patients with ESRD on hemodialysis (HD) were recruited randomly from a pool of 150 patients at the DaVita Hemodialysis Center (Boston, MA). The protocol was approved both by Institutional Review Boards of Boston University Medical Center and Massachusetts Institute of Technology. Informed consents were obtained and 10 ml of blood collected prior to the next HD session. Patients with Hb <8 gm/dl were excluded. Control sera matched for age-, gender- and ethnicity-matched subjects were obtained from Research Blood Component Inc. (Boston, MA). The controls with creatinine more than 1.0 mg/dl were excluded.

Generation of an indolic solute-specific thrombosis model: A group of 10-14 weeks old C57BL/6 male and female mice were administered with IS *ad libitum* in water and the excretion of IS was inhibited by Probenecid, an OAT1 and 3 channel inhibitor which suppresses the excretion of IS. First, different protocols, combining IS administration along with Probenecid were examined. IS dissolved in drinking water 4mg/ml and Probenecid 150 mg/kg IP twice daily yielded consistently high IS above 40-50 µg/ml, levels that are similar to patients with CKD stage 5/ESRD and was chosen for subsequent experiments. The serum IS levels were measured on day 0, 2, and 5 using LC/MS developed and validated for the measurement of IS in blood (**Fig. 1A**), after which the animals were subjected to ferric chloride-mediated carotid injury, which was performed, as described (*22*). Briefly, the right carotid artery was exposed in animals under isoflurane anesthesia, and basal blood flow recorded using a 0.5PSB S-series flow probe connected to a TS420 perivascular transit-time flow meter (Transonic, Ithaca, NY). The probe was removed, and a piece of Whatman filter paper (1 × 10mm) soaked in ferric chloride ($FeCl_3$) (Sigma-

Aldrich, St. Louis, MO) was placed under the carotid artery for 1 minute. After washing with warm physiological saline (0.9% NaCl), the probe was returned, and volume of blood flow was monitored for 20 minutes starting from the placement of the filter paper. Mean, maximum and minimum carotid flow was recorded using Powerlab Chart5 version 5.3 software, in one-second intervals. Time to occlusion was determined as the first measurement 0.299 mL/min. Average basal flow volume corresponds to an average of measurements over the 30 seconds preceding placement of the filter paper.

We first screened different concentrations of FeCL3 and one that resulted in time to occlusion (TtO) with minimum variation was chosen for further experiments (**fig. S4F**). The effects of AHR antagonist and YL-109 were examined in the following groups – **I**: Probenecid (control), **II**: IS + Probenacid, and **III**: IS + YL-109 (5 mg/kg IP). Group I**V** consisted of a single dose of Heparin given 2 hours prior to the procedure (10 units IP), which is known to prolong aPTT within therapeutic range (1.5-2.5 times control) (*37*).

Acknowledgments

The authors acknowledge Dr. Nigel Mackman (UNC, Chapel Hill) for his guidance in TF activity assay. We acknowledge Profs. David Salant and Nader Rahimi (Boston University School of Medicine- BUSM) for their scientific input. We thank Dr. Cam Patterson (University of North Carolina, Chapel Hill) for STUB1 KO and KI MEFs and wild-type and H260Q STUB1 constructs. We also thank Fernando García Polite, David Gómez Jiménez and Farran Lozano (Universitat Ramon Llull, Barcelona, Spain and MIT) for their technical assistance in flow loop experiments and Dan Mun for help in obtaining patient data for supplementary table 1. We thank Dr. Michael Kirber at the Imaging Core facilities of the Department of Medicine, BUMC for his assistance in confocal microscopy and analysis of the images. A part of this work was presented at the 2015 and 2016 American Society of Nephrology meetings.

Authors contributions: VCC and MS designed the research; MS, MEB, FA, KeR and SR performed the experiments; JH and MEB performed immunofluorescence studies; MS, MEB, SM and FA performed the animal experiments; AG provided the arteriovenous fistulae, KK, MB designed and performed the flow loop experiments; VBK performed quantitative histology and image processing; MO and KN synthesized YL-109 compound; RR assisted in the photochemical experiments, JF and AG provided scientific input and human tissue; MS, MEB and VCC prepared the figures; VCC; MS and MEB prepared the manuscript; DHS, JF, JMH, KK, VBK, ERE and KaR edited the manuscript.

Funding source:

This work was funded in part by NHLBI 1R01HL132325, Evans Faculty Merit award (VCC), NHLBI R01 HL080442 (KR), NIGMS R01 GM 49039 (ERE), P42 ES007381 and the Art BeCAUSE Breast Cancer Foundation (DHS), Hariri Research Award (#2016-10-009) from the Hariri Institute of Computing, Boston University and American Heart Association Young Scientist Development award (VBK), a Sharon Anderson Research Fellowship grant award from

American Society of Nephrology (MS), AHA Fellow to Faculty Transition grant 12FTF12080241 (KK), the grant SAF2013-43302-R from Spain Ministerio de Economía y Competitividad, and Fundació Empreses IQS (MB). A part of this work was funded by the Affinity Research Collaborative (ARC) program from the Department of Medicine, BUMC.

Disclosure

None

References:

1. G. Ocak, K. J. van Stralen, F. R. Rosendaal, M. Verduijn, P. Ravani, R. Palsson, T. Leivestad, A. J. Hoitsma, M. Ferrer-Alamar, P. Finne, J. De Meester, C. Wanner, F. W. Dekker, K. J. Jager, Mortality due to pulmonary embolism, myocardial infarction, and stroke among incident dialysis patients. *J Thromb Haemost* **10**, 2484-2493 (2012).
2. I. Iakovou, T. Schmidt, E. Bonizzoni, L. Ge, G. M. Sangiorgi, G. Stankovic, F. Airoldi, A. Chieffo, M. Montorfano, M. Carlino, I. Michev, N. Corvaja, C. Briguori, U. Gerckens, E. Grube, A. Colombo, Incidence, predictors, and outcome of thrombosis after successful implantation of drug-eluting stents. *JAMA* **293**, 2126-2130 (2005).
3. M. Shashar, J. Francis, V. Chitalia, Thrombosis in the uremic milieu--emerging role of "thrombolome". *Semin Dial* **28**, 198-205 (2015).
4. M. A. Crowther, C. M. Clase, P. J. Margetts, J. Julian, K. Lambert, D. Sneath, R. Nagai, S. Wilson, A. J. Ingram, Low-intensity warfarin is ineffective for the prevention of PTFE graft failure in patients on hemodialysis: a randomized controlled trial. *J Am Soc Nephrol* **13**, 2331-2337 (2002).
5. V. I. Patel, S. Mukhopadhyay, J. M. Guest, M. F. Conrad, M. T. Watkins, C. J. Kwolek, G. M. LaMuraglia, R. P. Cambria, Impact of severe chronic kidney disease on outcomes of infrainguinal peripheral arterial intervention. *J Vasc Surg* **59**, 368-375 (2014).
6. S. H. Park, W. Kim, C. S. Park, W. Y. Kang, S. H. Hwang, A comparison of clopidogrel responsiveness in patients with versus without chronic renal failure. *Am J Cardiol* **104**, 1292-1295 (2009).
7. V. C. Chitalia, S. Shivanna, J. Martorell, M. Balcells, I. Bosch, K. Kolandaivelu, E. R. Edelman, Uremic serum and solutes increase post-vascular interventional thrombotic risk through altered stability of smooth muscle cell tissue factor. *Circulation* **127**, 365-376 (2013).
8. M. B. Taubman, L. Wang, C. Miller, The role of smooth muscle derived tissue factor in mediating thrombosis and arterial injury. *Thromb Res* **122 Suppl 1**, S78-81 (2008).
9. J. Steffel, T. F. Luscher, F. C. Tanner, Tissue factor in cardiovascular diseases: molecular mechanisms and clinical implications. *Circulation* **113**, 722-731 (2006).
10. R. Vanholder, E. Schepers, A. Pletinck, E. V. Nagler, G. Glorieux, The uremic toxicity of indoxyl sulfate and p-cresyl sulfate: a systematic review. *J Am Soc Nephrol* **25**, 1897-1907 (2014).
11. S. Shivanna, K. Kolandaivelu, M. Shashar, M. Belghasim, L. Al-Rabadi, M. Balcells, A. Zhang, J. Weinberg, J. Francis, M. P. Pollastri, E. R. Edelman, D. H. Sherr, V. C. Chitalia, The Aryl Hydrocarbon Receptor is a Critical Regulator of Tissue Factor Stability and an Antithrombotic Target in Uremia. *J Am Soc Nephrol* **27**, 189-201 (2016).
12. D. I. Jalal, M. Chonchol, G. Targher, Disorders of hemostasis associated with chronic kidney disease. *Semin Thromb Hemost* **36**, 34-40 (2010).
13. S. S. Basra, P. Tsai, N. M. Lakkis, Safety and efficacy of antiplatelet and antithrombotic therapy in acute coronary syndrome patients with chronic kidney disease. *J Am Coll Cardiol* **58**, 2263-2269 (2011).
14. T. David, Y. C. Kim, L. K. Ely, I. Rondon, H. Gao, P. O'Brien, M. W. Bolt, A. J. Coyle, J. L. Garcia, E. A. Flounders, T. Mikita, S. R. Coughlin, Factor XIa-specific IgG and a reversal agent to probe factor XI function in thrombosis and hemostasis. *Sci Transl Med* **8**, 353ra112 (2016).

15. T. Petzold, M. Thienel, I. Konrad, I. Schubert, R. Regenauer, B. Hoppe, M. Lorenz, A. Eckart, S. Chandraratne, C. Lennerz, C. Kolb, D. Braun, J. Jamasbi, R. Brandl, S. Braun, W. Siess, C. Schulz, S. Massberg, Oral thrombin inhibitor aggravates platelet adhesion and aggregation during arterial thrombosis. *Sci Transl Med* **8**, 367ra168 (2016).
16. T. Gremmel, M. Muller, S. Steiner, D. Seidinger, R. Koppensteiner, C. W. Kopp, S. Panzer, Chronic kidney disease is associated with increased platelet activation and poor response to antiplatelet therapy. *Nephrol Dial Transplant* **28**, 2116-2122 (2013).
17. H. C. Yang, Y. Zuo, A. B. Fogo, Models of chronic kidney disease. *Drug Discov Today Dis Models* **7**, 13-19 (2010).
18. T. Kokubo, N. Ishikawa, H. Uchida, S. E. Chasnoff, X. Xie, S. Mathew, K. A. Hruska, E. T. Choi, CKD accelerates development of neointimal hyperplasia in arteriovenous fistulas. *J Am Soc Nephrol* **20**, 1236-1245 (2009).
19. B. Gondouin, C. Cerini, L. Dou, M. Sallee, A. Duval-Sabatier, A. Pletinck, R. Calaf, R. Lacroix, N. Jourde-Chiche, S. Poitevin, L. Arnaud, R. Vanholder, P. Brunet, F. Dignat-George, S. Burtey, Indolic uremic solutes increase tissue factor production in endothelial cells by the aryl hydrocarbon receptor pathway. *Kidney Int* **84**, 733-744 (2013).
20. S. Ito, M. Osaka, Y. Higuchi, F. Nishijima, H. Ishii, M. Yoshida, Indoxyl sulfate induces leukocyte-endothelial interactions through up-regulation of E-selectin. *J Biol Chem* **285**, 38869-38875 (2010).
21. S. K. Nigam, K. T. Bush, G. Martovetsky, S. Y. Ahn, H. C. Liu, E. Richard, V. Bhatnagar, W. Wu, The organic anion transporter (OAT) family: a systems biology perspective. *Physiol Rev* **95**, 83-123 (2015).
22. S. Matsuura, R. Mi, M. Koupenova, A. Eliades, S. Patterson, P. Toselli, J. Thon, J. E. Italiano, Jr., P. C. Trackman, N. Papadantonakis, K. Ravid, Lysyl oxidase is associated with increased thrombosis and platelet reactivity. *Blood* **127**, 1493-1501 (2016).
23. D. Kirchhofer, P. Moran, S. Bullens, F. Peale, S. Bunting, A monoclonal antibody that inhibits mouse tissue factor function. *J Thromb Haemost* **3**, 1098-1099 (2005).
24. B. D. Watson, W. D. Dietrich, R. Busto, M. S. Wachtel, M. D. Ginsberg, Induction of reproducible brain infarction by photochemically initiated thrombosis. *Ann Neurol* **17**, 497-504 (1985).
25. J. T. Paz, C. A. Christian, I. Parada, D. A. Prince, J. R. Huguenard, Focal cortical infarcts alter intrinsic excitability and synaptic excitation in the reticular thalamic nucleus. *J Neurosci* **30**, 5465-5479 (2010).
26. J. A. Jablonka, K. Burnat, O. W. Witte, M. Kossut, Remapping of the somatosensory cortex after a photothrombotic stroke: dynamics of the compensatory reorganization. *Neuroscience* **165**, 90-100 (2010).
27. Y. Miao, Z. Yu-Jie, W. Zhi-Jian, S. Dong-Mei, L. Yu-Yang, Z. Ying-Xin, G. Fei, Y. Shi-Wei, J. De-An, Chronic kidney disease and the risk of stent thrombosis after percutaneous coronary intervention with drug-eluting stents. *Catheter Cardiovasc Interv* **80**, 361-367 (2012).
28. G. Ocak, M. Verduijn, C. Y. Vossen, W. M. Lijfering, F. W. Dekker, F. R. Rosendaal, R. T. Gansevoort, B. K. Mahmoodi, Chronic kidney disease stages 1-3 increase the risk of venous thrombosis. *J Thromb Haemost* **8**, 2428-2435 (2010).

29. J. L. Morales, G. H. Perdew, Carboxyl terminus of hsc70-interacting protein (CHIP) can remodel mature aryl hydrocarbon receptor (AhR) complexes and mediate ubiquitination of both the AhR and the 90 kDa heat-shock protein (hsp90) in vitro. *Biochemistry* **46**, 610-621 (2007).
30. Q. Dai, C. Zhang, Y. Wu, H. McDonough, R. A. Whaley, V. Godfrey, H. H. Li, N. Madamanchi, W. Xu, L. Neckers, D. Cyr, C. Patterson, CHIP activates HSF1 and confers protection against apoptosis and cellular stress. *EMBO J* **22**, 5446-5458 (2003).
31. W. Xu, M. Marcu, X. Yuan, E. Mimnaugh, C. Patterson, L. Neckers, Chaperone-dependent E3 ubiquitin ligase CHIP mediates a degradative pathway for c-ErbB2/Neu. *Proc Natl Acad Sci U S A* **99**, 12847-12852 (2002).
32. M. T. Kirber, K. Chen, J. F. Keaney, Jr., YFP photoconversion revisited: confirmation of the CFP-like species. *Nat Methods* **4**, 767-768 (2007).
33. M. C. Riella, P. Roy-Chaudhury, Vascular access in haemodialysis: strengthening the Achilles' heel. *Nature reviews. Nephrology* **9**, 348-357 (2013).
34. S. Moshe, J. Siwak, U. Tapan, S. Y. Lee, R. D. Meyer, P. Parrack, J. Tan, F. Khatami, J. Francis, Q. Zhao, K. Hartshorn, V. B. Kolachalama, N. Rahimi, V. Chitalia, c-Cbl mediates the degradation of tumorigenic nuclear beta-catenin contributing to the heterogeneity in Wnt activity in colorectal tumors. *Oncotarget* **7**, 71136-71150 (2016).
35. K. Kolandaivelu, B. B. Leiden, E. R. Edelman, Predicting response to endovascular therapies: dissecting the roles of local lesion complexity, systemic comorbidity, and clinical uncertainty. *J Biomech* **47**, 908-921 (2014).
36. H. Hiyoshi, N. Goto, M. Tsuchiya, K. Iida, Y. Nakajima, N. Hirata, Y. Kanda, K. Nagasawa, J. Yanagisawa, 2-(4-Hydroxy-3-methoxyphenyl)-benzothiazole suppresses tumor progression and metastatic potential of breast cancer cells by inducing ubiquitin ligase CHIP. *Sci Rep* **4**, 7095 (2014).
37. Y. Li, J. F. Sun, X. Cui, H. Mani, R. L. Danner, X. Li, J. W. Su, Y. Fitz, P. Q. Eichacker, The effect of heparin administration in animal models of sepsis: a prospective study in Escherichia coli-challenged mice and a systematic review and metaregression analysis of published studies. *Crit Care Med* **39**, 1104-1112 (2011).
38. J. Loscalzo, Venous thrombosis in the nephrotic syndrome. *N Engl J Med* **368**, 956-958 (2013).
39. A. Bertelli, A. A. Bertelli, G. Galmozzi, L. Giovannini, M. Mian, Thrombosis induced by endothelin (ET-1) and carrageenin in rats treated with indomethacin and propionyl carnitine. *Drugs Exp Clin Res* **19**, 75-78 (1993).
40. T. Jia, H. Olauson, K. Lindberg, R. Amin, K. Edvardsson, B. Lindholm, G. Andersson, A. Wernerson, Y. Sabbagh, S. Schiavi, T. E. Larsson, A novel model of adenine-induced tubulointerstitial nephropathy in mice. *BMC Nephrol* **14**, 116 (2013).
41. O. Volovelsky, G. Cohen, A. Kenig, G. Wasserman, A. Dreazen, O. Meyuhas, J. Silver, T. Naveh-Many, Phosphorylation of Ribosomal Protein S6 Mediates Mammalian Target of Rapamycin Complex 1-Induced Parathyroid Cell Proliferation in Secondary Hyperparathyroidism. *J Am Soc Nephrol* **27**, 1091-1101 (2016).
42. D. Molino, D. De Lucia, N. Gaspare De Santo, Coagulation disorders in uremia. *Semin Nephrol* **26**, 46-51 (2006).

43. K. A. Fox, E. M. Antman, G. Montalescot, S. Agewall, B. SomaRaju, F. W. Verheugt, J. Lopez-Sendon, H. Hod, S. A. Murphy, E. Braunwald, The impact of renal dysfunction on outcomes in the ExTRACT-TIMI 25 trial. *J Am Coll Cardiol* **49**, 2249-2255 (2007).
44. A. J. Kirtane, G. Piazza, S. A. Murphy, D. Budiu, D. A. Morrow, D. J. Cohen, E. Peterson, N. Lakkis, H. C. Herrmann, T. M. Palabrica, C. M. Gibson, T. S. Group, Correlates of bleeding events among moderate- to high-risk patients undergoing percutaneous coronary intervention and treated with eptifibatide: observations from the PROTECT-TIMI-30 trial. *J Am Coll Cardiol* **47**, 2374-2379 (2006).
45. K. P. Alexander, A. Y. Chen, M. T. Roe, L. K. Newby, C. M. Gibson, N. M. Allen-LaPointe, C. Pollack, W. B. Gibler, E. M. Ohman, E. D. Peterson, C. Investigators, Excess dosing of antiplatelet and antithrombin agents in the treatment of non-ST-segment elevation acute coronary syndromes. *JAMA* **294**, 3108-3116 (2005).
46. P. Muller, E. Ruckova, P. Halada, P. J. Coates, R. Hrstka, D. P. Lane, B. Vojtesek, C-terminal phosphorylation of Hsp70 and Hsp90 regulates alternate binding to co-chaperones CHIP and HOP to determine cellular protein folding/degradation balances. *Oncogene* **32**, 3101-3110 (2013).
47. N. A. Blessing, A. L. Brockman, D. N. Chadee, The E3 ligase CHIP mediates ubiquitination and degradation of mixed-lineage kinase 3. *Mol Cell Biol* **34**, 3132-3143 (2014).
48. A. Ciechanover, The unravelling of the ubiquitin system. *Nature reviews. Molecular cell biology* **16**, 322-324 (2015).
49. N. Mackman, Triggers, targets and treatments for thrombosis. *Nature* **451**, 914-918 (2008).
50. L. Dou, E. Bertrand, C. Cerini, V. Faure, J. Sampol, R. Vanholder, Y. Berland, P. Brunet, The uremic solutes p-cresol and indoxyl sulfate inhibit endothelial proliferation and wound repair. *Kidney Int* **65**, 442-451 (2004).
51. P. Boccardo, G. Remuzzi, M. Galbusera, Platelet dysfunction in renal failure. *Semin Thromb Hemost* **30**, 579-589 (2004).
52. U. Windberger, A. Bartholovitsch, R. Plasenzotti, K. J. Korak, G. Heinze, Whole blood viscosity, plasma viscosity and erythrocyte aggregation in nine mammalian species: reference values and comparison of data. *Exp Physiol* **88**, 431-440 (2003).
53. K. Kolandaivelu, R. Swaminathan, W. J. Gibson, V. B. Kolachalama, K. L. Nguyen-Ehrenreich, V. L. Giddings, L. Coleman, G. K. Wong, E. R. Edelman, Stent thrombogenicity early in high-risk interventional settings is driven by stent design and deployment and protected by polymer-drug coatings. *Circulation* **123**, 1400-1409 (2011).
54. K. Kolandaivelu, E. R. Edelman, Environmental influences on endovascular stent platelet reactivity: an in vitro comparison of stainless steel and gold surfaces. *J Biomed Mater Res A* **70**, 186-193 (2004).
55. I. A. Murray, G. Krishnegowda, B. C. DiNatale, C. Flaveny, C. Chiaro, J. M. Lin, A. K. Sharma, S. Amin, G. H. Perdew, Development of a selective modulator of aryl hydrocarbon (Ah) receptor activity that exhibits anti-inflammatory properties. *Chem Res Toxicol* **23**, 955-966 (2010).
56. L. F. Casserly, L. M. Dember, Thrombosis in end-stage renal disease. *Semin Dial* **16**, 245-256 (2003).

57. C. D. Ke Yang, Xinmiao Wang, Fengju Li, Yang Xu, Song Wang, Shilei Chen, Fang Chen, Mingqiang Shen, Mo Chen, Mengjia Hu, Ting He, Yongping Su, Junping Wang, Jinghong Zhao, Uremic solute indoxyl sulfate-induced platelet hyperactivity contributes to CKD-associated thrombosis in mice. *Blood*, (2017).
58. R. K. Zhang A, , Ng Seng Kah, Ravid K and Chitalia V, A Mass Spectrometric Method for Quantification of Tryptophan-Derived Uremic Solutes in Human Serum *Journal of Biological Methods* **epub**, (2017).
59. K. Kolandaivelu, E. R. Edelman, Low background, pulsatile, in vitro flow circuit for modeling coronary implant thrombosis. *J Biomech Eng* **124**, 662-668 (2002).
60. V. B. Kolachalama, A. R. Tzafriri, D. Y. Arifin, E. R. Edelman, Luminal flow patterns dictate arterial drug deposition in stent-based delivery. *J Control Release* **133**, 24-30 (2009).
61. D. Bluestein, G. Girdhar, S. Einav, M. J. Slepian, Device thrombogenicity emulation: a novel methodology for optimizing the thromboresistance of cardiovascular devices. *J Biomech* **46**, 338-344 (2013).
62. D. M. Wootton, D. N. Ku, Fluid mechanics of vascular systems, diseases, and thrombosis. *Annu Rev Biomed Eng* **1**, 299-329 (1999).

Figure legend:

Figure 1. IS mediates the hyperthrombotic uremic phenotype in an AHR-and TF-dependent manner across all CKD stages

(a) Generation of an indolic solute-specific animal model with IS levels corresponding to levels in patients with advanced CKD. For this and all the animal experiments, 10-14 week-old C57BL/6 male and female mice were used. Blood from these animals was exposed to a combination of Probenecid and IS and were analyzed using LC/MS (*58*). The dotted line corresponds to the average IS levels in ESRD patients (40-60 µg/ml) (*11*). Probenecid and sham injected animals (Controls) served as controls. p value corresponds to a significant increase in serum IS levels in the Probenecid + IS group compared to the Probenecid group alone. An average of 5 animals per time point is shown. Error bar = SD. No significant difference in IS levels were observed between male and female mice.

(b) The pattern of carotid artery blood flow with occlusion. An ultrasound probe measured carotid artery flow in animals, which was noted to be 1.25-2 ml/min. The flow was monitored for 20 minutes after the application of a 10% $FeCL_3$ strip. The time until the blood flow took to drop 0-0.299 ml/min was considered as Time to Occlusion (TtO) and is shown by an arrow. TtO shortened with IS, was reversed with the co-administration of CH223191, an AHR antagonist. A representative carotid artery blood flow reading from a total of eight animals per group is shown. No significant difference in response was observed between male and female mice.

(c) Validation of $FeCl_3$ injury model in uremic *milieu*. Hematoxylin and eosin stained sections of carotid arteries harvested after the $FeCl_3$ procedure are shown. Representative images from six vessels per group are shown. Control left (LT) carotid artery showed blood in the lumen, while the $FeLC_3$ exposed right carotid (RT) showed a large thrombus occupying the lumen. Scale bar = 25 µm.

(d) IS induces hyperthrombotic *milieu* in an AHR-dependent manner. The TtO was compared in three groups after 5 days of exposure to different agents. An average of TtO from eight animals per group is shown. Error bars = SD. No significant difference in TtO was observed between male and female mice.

(e) IS induces thrombosis in a TF-dependent manner. A group of 12 mice were exposed to Probenecid + IS for five days followed by the $FeCl_3$ carotid artery thrombosis assay. Half an hour prior to the assay, the animals were given the control antibody (IP 20 mg/kg rat anti-mouse) or rat anti-mouse anti-TF neutralizing antibody (IP 20 mg/kg). An average TtO from six animals per group is shown. Error bars = SEM.

(f) IS-enhanced thrombogenicity validated in a photochemical thrombosis model. Two groups of animals received a single intravenous injection of Rose Bengal dye. The carotid artery was then illuminated with broad-spectrum light to induce thrombosis. The average TtO from six animals per group is shown. Error bars = SEM.

(g) IS mediates the hyperthrombotic *milieu* across all the stages of CKD. A total of 16 animals exposed to Probenecid with or without IS in water ranging from 0-4 mg/ml for a total of 5 days were subjected to the carotid artery thrombosis assay and IS measurement in blood at the time of the procedure. Each point represents an individual animal. Pearson correlation coefficient between IS and TtO was $R = -0.87$ and $p < 0.001$, which supports a significant inverse correlation between IS levels and thrombosis. Average IS levels in human patients at different stages of CKD are shown (*3, 11*).

Figure 2. STUB1 destabilizes and ubiquitinates TF and mediates TF regulation by AHR.

(**a**). Doubling of TF expression with *STUB1* silencing in vSMCs. Lysates from primary human aortic vascular smooth muscle cells (vSMCs) transfected with control (Csi) or *STUB1* silencing oligos (*STUB1si*) were probed for TF and STUB1 and normalized to loading control (GAPDH). Because of proximity in molecular weights, separate blots run in parallel on the same samples were probed for loading control (GAPDH), a strategy that is also applied to other figures. A representative blot of four independent experiments is shown. TF levels more than doubled ($p = 0.001$) with *STUB1si* compared to *Csi*.

(**b**). *STUB1* silencing significantly increases surface procoagulant TF activity. Overnight serum starved vSMCs pre-transfected with *control* (Csi) and *STUB1* sioligos (*STUB1si*) were stimulated with 5% calf serum, control or uremic human serum for 24 hours. An average of two independent experiments performed in duplicates is shown. # p value showed significantly higher TF activity in Csi vSMCs treated with uremic serum compared to control serum. * p values showed significantly higher TF activity in *STUB1* silenced vSMCs under all the conditions compared to Csi vSMCs. Error bars = SD.

(**c**) Loss of *STUB1* activity stabilizes TF. vSMCs lysates transfected with control (*Cs*i) and STUB1 silencing oligos (*STUB1si*) grown in 5% uremic serum for 24 hours and then treated with the protein translation blocker cycloheximide (80 μM) for the indicated time. The amount of remaining TF, as detected by Western blotting, indicates its stability. Equal amounts of lysates were probed separately to confirm *STUB1* silencing. Because of proximity in molecular weights, separate blots run in parallel on the same sample (and same lysate volume) were probed for loading control (anti-GAPDH). A representative figure from four independent experiments is shown.

(**d**) *STUB1* silencing significantly prolongs the half-life of TF. Densitometry of normalized TF bands performed using ImageJ represented as the percentage of TF at time 0 is shown. The time to reach 50% of initial TF was considered as the half-life of TF. An average of four experiments is shown. TF levels were significantly higher upon *STUB1* silencing at the end of 4 hours (average TF at 4 hours in *Contro*l si was 38.7% of time zero and *STUB1* si was 65.7% of time zero, p value < 0.001) and at the end of 8 hours (average TF in Control si was 20.7% and *STUB1* si was 56.2% of TF levels at time zero, p value < 0.001). Error bars = SD.

(e). *STUB1* mediates TF downregulation by an AHR antagonist. vSMCs pretransfected with control (*Csi*) and STUB1 sioligos (*STUB1si*) were treated with 5% uremic serum with or without the AHR antagonist CB7993113 (20 μM) for 24 hours, followed by Western blotting. Because of proximity in molecular weights, separate blots run in parallel on the same sample (and same lysate volume) were probed for loading control (anti-tubulin). A representative of two independent experiments done in duplicates is shown.

(**f**) *STUB1* silencing reduces AHR antagonist-mediated TF ubiquitination in the uremic *milieu*. vSMCs lysates were retransfected with control (*Csi*) and *STUB1* silencing oligos (*STUB1si*), treated with 5% uremic serum + 20 μM of CB7993113 for 12 hours and 10 μM MG132 for 4 hours, were immunoprecipitated with anti-TF antibody and probed with anti-ubiquitin antibody. Five percent of whole cell lysates are shown as inputs. A representative of three independent experiments is shown.

Figure 3. A dynamic STUB1-TF interaction dependent on the uremic status.

(**a**) Purified recombinant GST-tagged STUB1 directly interacts with recombinant human TF. Recombinant GST-tagged STUB1 protein immobilized on GST beads and treated with recombinant human lipidated TF protein for 4 hours at 4^{o} C. The eluents were probed by Western blotting for TF. Five percent of recombinant GST-tagged STUB1 stained with Commassie and recombinant TF are shown as inputs. A representative immunoblot from four independent experiments is shown.

(**b**) STUB1-TF interaction is reduced in uremic *milieu* and enhanced with AHR antagonist. vSMCs pretreated with 10 µM of IS for 24 hours and/or 20 µM of CH223191 for 20 minutes followed by IP using anti-STUB1 antibody and eluents probed for TF. The stripped blot was reprobed for STUB1 to compare the IPed STUB1 as controls. Five percent of cell lysates are shown as inputs. A representative blot from three independent experiments is shown.

(**c**) Deletion of C-terminus tail of TF compromises its interaction with STUB1. HEK293T cells stably expressing Flag-tagged wild-type TF (TF WT) or TF C-terminus truncation (TFdelC) were transfected with Myc-tagged STUB1. The cell lysates were immunoprecipitated with Flag-tag or Myc-tag antibodies and co-IPed proteins were detected using reciprocal antibodies. Five percent of lysates were probed as inputs. STUB1 binds to the TF wild-type but not TFdelC. A representative of two independent experiments done in duplicates is shown.

(**d**) STUB1 destabilizes wild-type (WT) TF. HEK293T cells co-expressing Flag-tagged WT TF and empty vector (control) or Myc-tagged STUB1 plasmid were treated with 80 µM cycloheximide to block the protein translation for indicated amount of time. The TF bands were normalized and equal amounts of lysates showed Myc-tag STUB1 expression as controls. Because of proximity in molecular weights, separate blots run in parallel on the same samples were probed for loading control (GAPDH). A representative from three independent experiments is shown.

(**e**) STUB1 fails to destabilize TF truncation lacking C-terminus. HEK293T cells co-expressing Flag-tagged TF delC and empty vector (control) or Myc-tagged STUB1 were processed as above. A representative from three independent experiments is shown.

(**f**) STUB1 enhances ubiquitination of WT TF but not of the TF truncation lacking the C-terminus. HEK293T cells co-expressing Flag-tag TF-WT or TF delC (delC) along with Myc-tag STUB1 were treated with 10 μM MG132 for 16 hours. The lysates were immunoprecipitated with anti-TF antibodies and probed for ubiquitin (Ub). The stripped blot was reprobed with Flag-tag. Five percent of the cell lysates are shown as controls. A representative immunoblot from three independent biological experiments is shown.

(**g**) STUB1 and TF exhibit opposite expression patterns in an arteriovenous fistula (AVF) of a CKD patient. Confocal images of paraffin-embedded sections of an explanted AVF from a 42-year-old male with CKD stage 5 patient stained with anti-TF and anti-STUB1 antibodies are shown. In the same AVF, different regions show higher TF and lower STUB1 expression (area 1) and vice versa (area 2). Representatives of eight immunofluorescence images acquired from four CKD/end stage renal disease ESRD patients are shown (Supplementary table 1). Scale bar = 100 μM.

(**h**) Overview of the image-processing pipeline for quantifying the expression levels of and relationship between STUB1 and TF. An object recognition algorithm was developed to correlate cell-level intensity distributions of STUB1 with TF. The pipeline consisted of the following steps: basic image pre-processing, size-based morphology filtering and object-level intensity correlation (Methods for more details).

(**i**) An inverse correlation between STUB1 and TF expressions in human AVF. Eight random immunofluorescence images from four explanted AVFs from CKD/ESRD patients were analyzed using an object recognition algorithm. The intensities of TF and STUB1 within image objects containing vSMCs (average of 187 cells/image, total 1501 cells) were quantified and

averaged per image. A linear fit with R^2 = 0.54 and a negative Spearman coefficient support an inverse correlation between STUB1 and TF in uremic vessels. Error bars = SD.

(**j**) Reduced STUB1-TF co-localization in vSMCs of uremic compared to non-uremic vessels. Confocal images of paraffin-embedded sections of an explanted AVF from a 47-year old CKD patient (uremic) and a popliteal artery from a 53-year old male with normal renal function (non-uremic) were stained with anti-TF and anti-STUB1 antibodies. Two representatives from a total of eight uremic and non-uremic images are shown. L = lumen, S = subendothelium, M = media. Scale bar = 100 μm.

(**k**) STUB1-TF co-localization is significantly reduced in vSMCs of uremic compared to non-uremic vessels. Confocal images acquired randomly from four explanted arteriovenous fistulae from CKD/ESRD patients and popliteal arteries from patients with normal renal function were analyzed using a pixel level co-localization algorithm. Percentage co-localization of TF-STUB1 defined by the fraction of pixels with intensity values greater than image-specific thresholds for STUB1 and TF and was compared between two groups. Error bars = SD

Figure 4. STUB1 modulation regulates TF activity and thrombosis in a post-vascular interventional model.

(a). Scheme of flow loop preparation. Fibronectin-coated silastic tubes were seeded overnight with vSMCs and exposed to IS or uremic serum for 16 hours before loading on the flow loop platform.

(b). Flow loop model. The flow loop system consists of silastic loops with a reactive segment lined by the monolayer of vSMCs or MEFs loaded on rotor-stages driven by motors and motion controllers. The entire rotor system held within an incubator at 37^0 C is connected remotely to the controllers, circuitry and flow recorders. The tubes injected with the human blood were subjected to coronary flow pattern until clotting appears. The wall motion creates bi-directional flows that are measured via onboard, extracorporeal flow probes built into the rotor stages.

(**c**) Higher thrombogenicity of *STUB1* KO cells compared to WT cells. STUB1 WT and KO MEFs seeded on fibronectin-coated tubes were subjected to the flow loop experiment, as described above. A tube from six independent flow loops in each group is shown.

(**d)**. Loss of *STUB1* activity significantly increases the clot burden in a post-interventional thrombosis model. Average hemoglobin (Hb) and lactic dehydrogenase (LDH) values of the thrombi from flow loops lined with STUB1 KO and WT MEFs are shown. Average results from six independent tubes are shown. Error bars = SEM.

(**e**) (Upper panel) YL-109. 2-(4-Hydroxy-3-methoxyphenyl)- benzothiazole is a recently described STUB1 enhancer through an increase in *STUB1* transcription (*36*). (Lower panel) YL-109 inhibits IS-mediated thrombogenicity in a post-interventional vascular model. Primary human aortic vSMCs seeded on fibronectin-coated tubes and serum starved overnight were stimulated with IS (10 μM) with or without YL-109 25 μM for 24 hours before loading on to the flow loops. A tube from six independent flow loops in each group is shown.

(**f**) YL-109 significantly inhibits clot burden in a post-interventional thrombosis model. Hb and LDH contents of the thrombi from flow loops pretreated with IS with or without YL-109 are shown. Average values from six tubes are shown. Error bars = SEM.

(**g**) YL-109 increases STUB1 and inhibits uremia-induced TF levels. Lysates of vSMCs pretreated with 5% uremic serum along with indicated amount of YL-109 for 24 hours were probed by Western blotting for TF and STUB1. Because of proximity in molecular weights, separate blots run in parallel on the same sample (and same lysate volume) were probed for loading control (tubulin). Representative blots from three independent experiments are shown.

(**h**) YL-109 inhibits uremic serum-induced TF activity in a dose-dependent manner. Serum starved confluent monolayer of vSMCs treated with 5% uremic serum and YL-109 at different concentrations and TF activity measured in pM and normalized to 10^3 cells. An average of two independent experiments performed in duplicates is shown. A log dose of YL-109 was plotted against TF activity and a significant inhibition in TF activity was observed at different concentrations of YL-109. Error bars = SD.

(**i**) TF ubiquitination is enhanced by YL-109 in the presence of IS. Primary human aortic vSMCs were co-transfected with the Flag-tag TF and HA-tag-ubiquitin and were treated with IS (50 uM) with or without YL-109 (20 uM) for 24 hours, and with MG132 (5 uM) for 16 hours before harvest. The cells were lyzed using RIPA buffer and incubated for four hours with Flag-tag antibody followed by treatment of protein A/G agarose beads for four hours at 4^0c. The eluents were resolved on SDS-PAGE gel and the blot was probed using HA antibody. Five percent of whole cell lysates were separately probed for STUB1. A representative blot of three independent experiments is shown.

Figure 5. YL-109 normalizes the hyperthrombotic uremic phenotype without altering the bleeding risk.

(**a**) The experimental design assessing the effect of YL-109 on IS-specific thrombosis model. Animal groups were exposed to a combination of Probenecid and IS along with the indicated compound (5 mg/kg of YL-109) once a day for 5 days as indicated. A single dose of Heparin that increases aPTT in therapeutic range (*37*) was given IP two hours prior to the procedure. The animals were subjected to the carotid artery thrombosis model using 10% $FeCL_3$.

(**b**) IS-mediated shortened time to occlusion (TtO) is prolonged by YL-109. The baseline carotid artery blood flow of 1.25-1.5 ml/min was detected using an ultrasound probe and the time to reduce the flow to baseline 0-0.2 ml/min was considered as the time to occlusion (TtO), which was the primary end point of the study. A representative flow pattern from each group from the following experiment (Fig. 5C) is shown.

(**c**) IS-mediated thrombosis is normalized to the non-uremic range with YL-109, unlike Heparin. Average of TtO from each group of animals from three independent experiments is shown. A total 35 animals were used for this study. Probenecid, N = 9; Probenecid + IS, N = 12; Probenecid + IS + YL-109, N = 8; Probenecid + IS + Heparin, N = 6. Compared to IS (CKD group), the TtO was significantly increased with YL-109. However, compared to the Probenecid controls (non-CKD group), no significant difference in TtO was observed with YL-109 ($p = 0.65$). On the other hand, Heparin significantly prolonged TtO compared to both IS ($p = 0.001$) and Probenecid control groups ($p = 0.021$). Error bars = SD.

(**d**). A significant increase in STUB1 and reduction in TF in the aortas of YL-109 exposed animals. The aortas of the animals harvested in RIPA buffer and sonicated were probed. TF and STUB1 expressions were normalized to the loading controls. Average of normalized TF and

STUB1 expressions in the aortas of five mice injected with IS with or without YL-109 are shown. Error bars = SD.

(**e**) A significant inverse correlation between TF reduction in the aortas of YL-109 treated animals and the prolongation of TtO. TF was examined in the lysates of the aortas of IS treated animals. The average TF from this group was used to normalize the changes in the TF levels in individual aorta of animals treated with YL-109 + IS. A similar strategy yielded the changes in TtO in seven individual YL-109 + IS- treated animals. Changes in TF levels in aortas of YL-109-treated animals and their respective TtO was plotted (Spearman rho = -0.833 and p = 0.02).

(**f**) Increase in IS levels in Adenine CKD model corresponding to the levels in patients with advanced CKD. IS levels in blood obtained from animals exposed to 0.25% Adenine diet for two weeks, measured using LC/MS, were compared to levels in animals on regular diet (control). An average of data obtained from five mice per group is shown. Error bars = SD. N = 5 animals/group

(**g**). Enhanced thrombogenicity in Adenine-induced CKD model was reversed to the non-CKD range with AHR inhibitor (CH223191) or STUB1 enhancer (YL-109). The indicated groups of animals exposed to two weeks of 0.25% Adenine diet were subjected to FeCL3-induced thrombosis at the end of two weeks treatment. The animals received CH223191 (10 mg/kg IP) or YL-109 (5 mg/kg IP) for five days prior to the thrombosis assay. The mice on regular diet served as controls. An average of five mice per group is shown. The p value for the Adenine group was obtained by comparing to the animals on regular diet (control) and the p values of CH223191 and YL-109 groups were obtained by comparing to the Adenine group. Error bars = SEM.

(**h**) YL-109, unlike Heparin, does not alter the tail vein bleeding time compared to the Probenecid controls. An average bleeding time from five mice per group is shown. Error bars =

SD. Compared to the Probenecid controls (non-CKD), the bleeding time did not differ with YL-109, in contrast to Heparin, which significantly prolonged the bleeding time.

(i) YL-109 reverts the uremic hyperthrombotic phenotype to non-CKD range without altering the hemostatic balance. The differences between the average tail vein bleeding times (on Y-axis) and TtO between Probenecid control (non-CKD) and different groups are shown. The solid line represents the average bleeding time of the Probenecid control group, and the dotted lines represent two times the SD of bleeding time of the same group. The shaded areas are the regions 2SD beyond of the bleeding time of the Probenecid control.

Figure 1

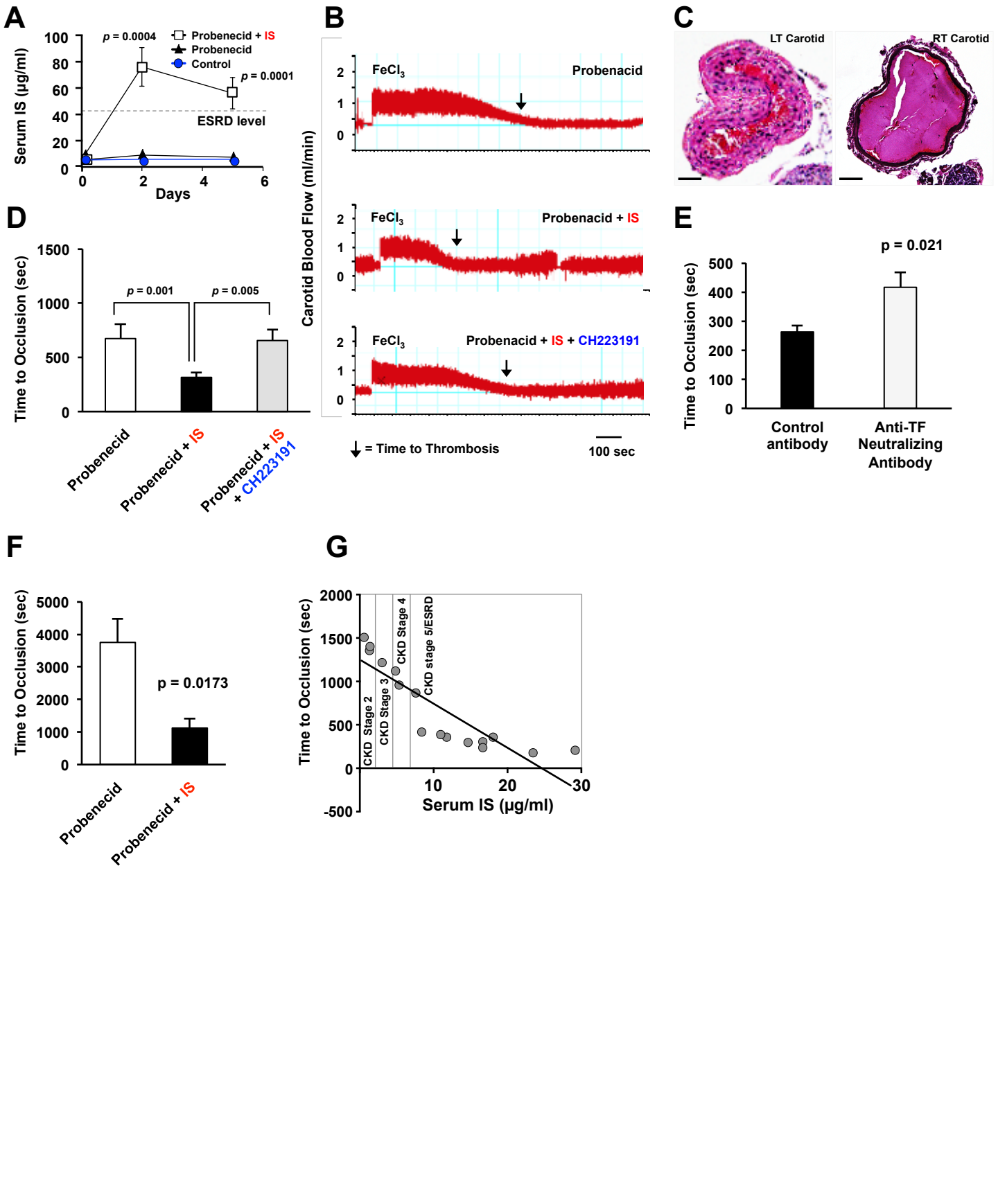
A
Serum IS (μg/ml)
Days
p = 0.0004
p = 0.0001
Probenecid + IS
Probenecid
Control
ESRD level
B
Carotid Blood Flow (ml/min)
FeCl3
Probenacid
Probenacid + IS
Probenacid + IS + CH223191
= Time to Thrombosis
100 sec
C
LT Carotid
RT Carotid
D
Time to Occlusion (sec)
p = 0.001
p = 0.005
Probenecid
Probenecid + IS
Probenecid + IS + CH223191
E
Time to Occlusion (sec)
p = 0.021
Control antibody
Anti-TF Neutralizing Antibody
F
Time to Occlusion (sec)
p = 0.0173
Probenecid
Probenecid + IS
G
Time to Occlusion (sec)
Serum IS (μg/ml)
CKD Stage 2
CKD Stage 3
CKD Stage 4
CKD stage 5/ESRD

Figure 2

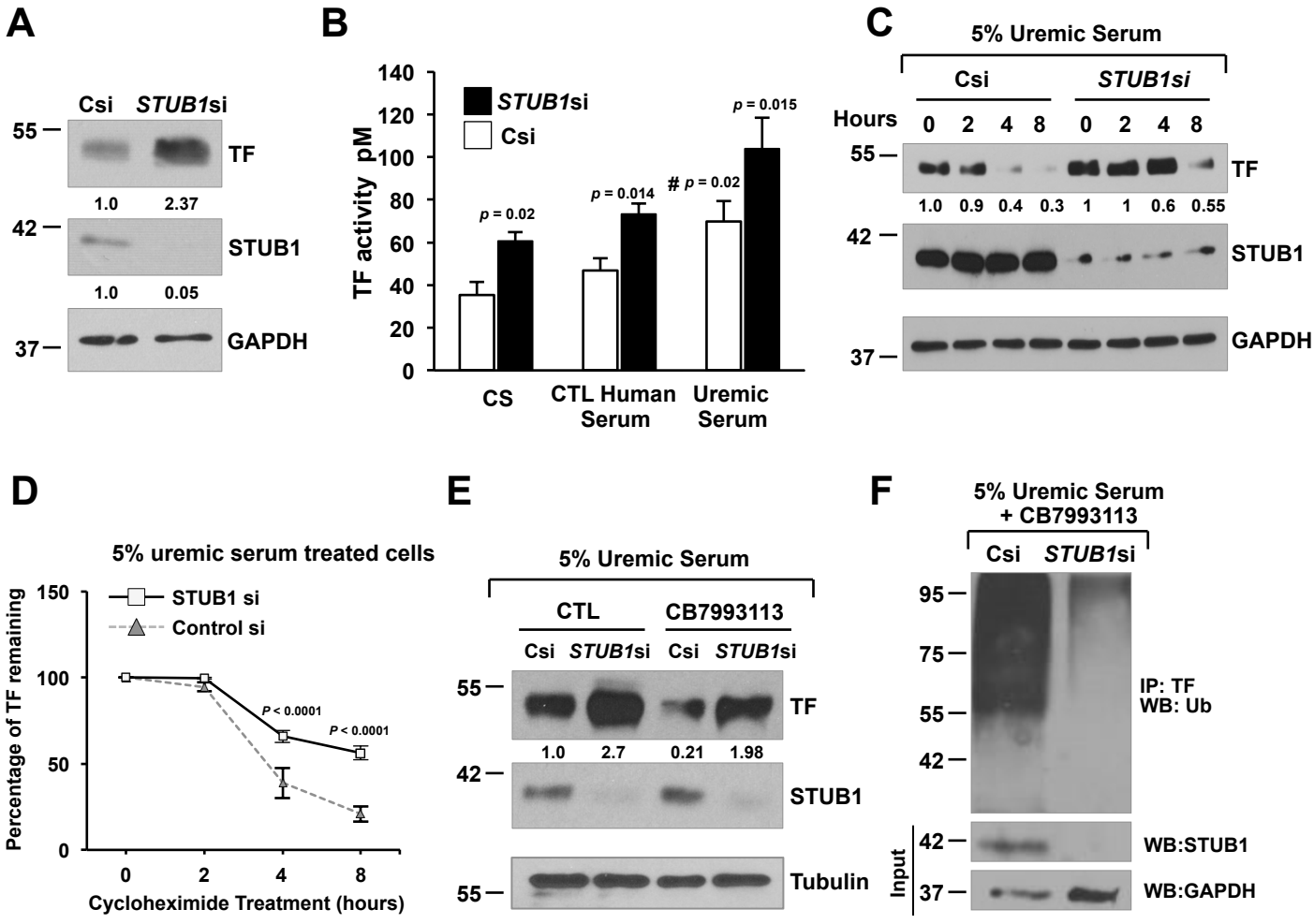
A
Csi
STUB1si
55
TF
1.0
2.37
42
STUB1
1.0
0.05
37
GAPDH
B
STUB1si
Csi
TF activity pM
140
120
100
80
60
40
20
0
p = 0.02
p = 0.014
# p = 0.02
p = 0.015
CS
CTL Human Serum
Uremic Serum
C
5% Uremic Serum
Csi
STUB1si
Hours
0 2 4 8 0 2 4 8
55
TF
1.0 0.9 0.4 0.3 1 1 0.6 0.55
42
STUB1
37
GAPDH
D
5% uremic serum treated cells
STUB1 si
Control si
Percentage of TF remaining
150
100
50
0
P < 0.0001
P < 0.0001
0
2
4
8
Cycloheximide Treatment (hours)
E
5% Uremic Serum
CTL
CB7993113
Csi
STUB1si
Csi
STUB1si
55
TF
1.0
2.7
0.21
1.98
42
STUB1
55
Tubulin
F
5% Uremic Serum
+ CB7993113
Csi
STUB1si
95
75
55
42
IP: TF
WB: Ub
Input
42
WB:STUB1
37
WB:GAPDH

Figure 3

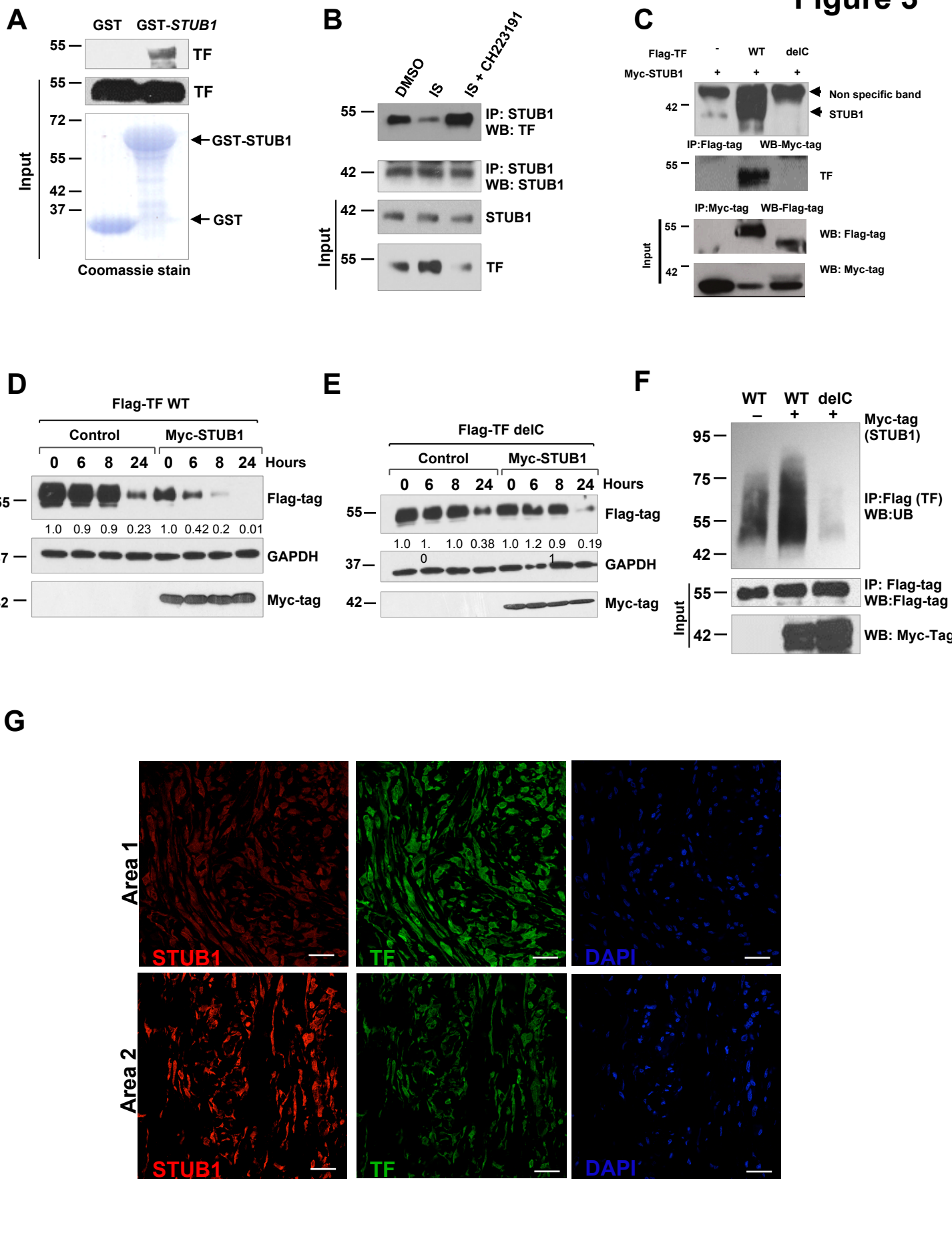
A
GST
GST-STUB1
55
TF
55
TF
72
55
42
37
Input
GST-STUB1
GST
Coomassie stain
B
DMSO
IS
IS + CH223191
55
IP: STUB1
WB: TF
42
IP: STUB1
WB: STUB1
42
STUB1
Input
55
TF
C
Flag-TF
-
WT
delC
Myc-STUB1
+
+
+
42
Non specific band
STUB1
IP:Flag-tag
WB-Myc-tag
55
TF
IP:Myc-tag
WB-Flag-tag
Input
55
WB: Flag-tag
42
WB: Myc-tag
D
Flag-TF WT
Control
Myc-STUB1
0 6 8 24 0 6 8 24 Hours
55
Flag-tag
1.0 0.9 0.9 0.23 1.0 0.42 0.2 0.01
37
GAPDH
42
Myc-tag
E
Flag-TF delC
Control
Myc-STUB1
0 6 8 24 0 6 8 24 Hours
55
Flag-tag
1.0 1. 1.0 0.38 1.0 1.2 0.9 0.19
0
1
37
GAPDH
42
Myc-tag
F
WT
WT
delC
–
+
+
95
Myc-tag
(STUB1)
75
55
IP:Flag (TF)
WB:UB
42
Input
55
IP: Flag-tag
WB:Flag-tag
42
WB: Myc-Tag
G
Area 1
STUB1
TF
DAPI
Area 2
STUB1
TF
DAPI

Figure 3

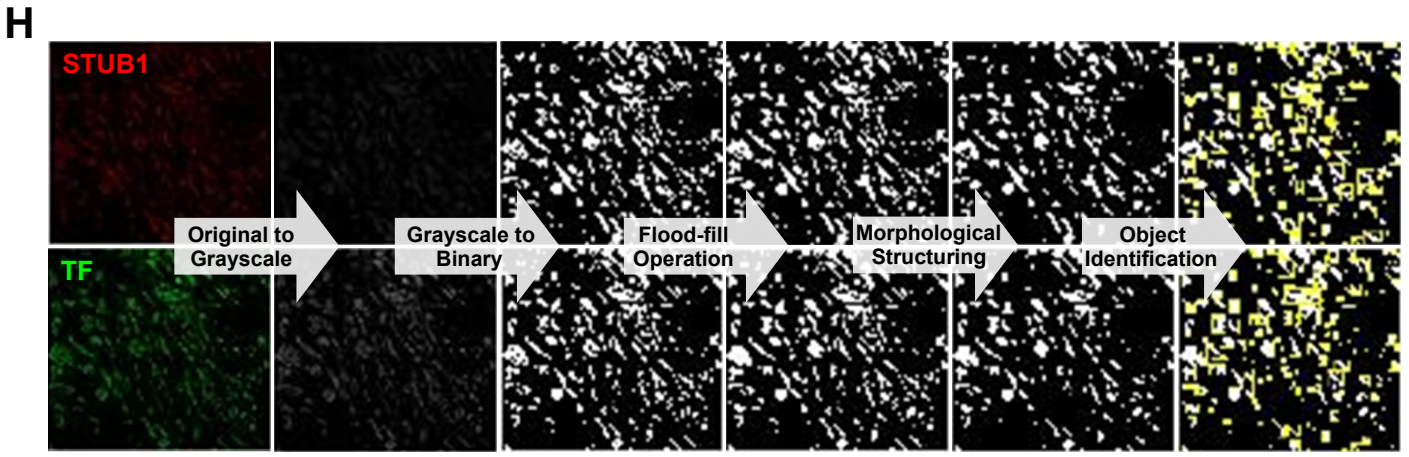
H
STUB1
TF
Original to Grayscale
Grayscale to Binary
Flood-fill Operation
Morphological Structuring
Object Identification

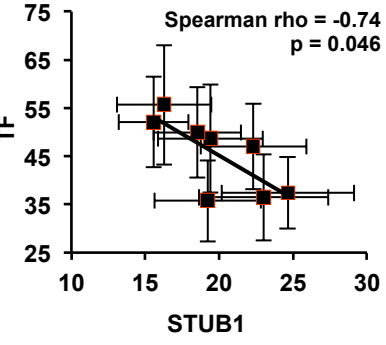
I
Spearman rho = -0.74
p = 0.046
75
65
55
45
35
25
10
15
20
25
30
STUB1
TF

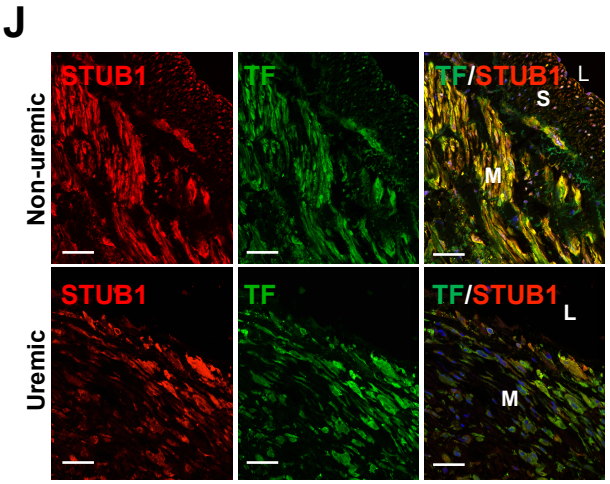
J
Non-uremic
Uremic
STUB1
TF
TF/STUB1
L
S
M

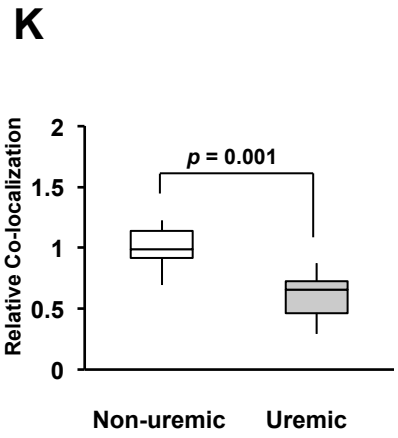
K
Relative Co-localization
p = 0.001
2
1.5
1
0.5
0
Non-uremic
Uremic

Figure 4

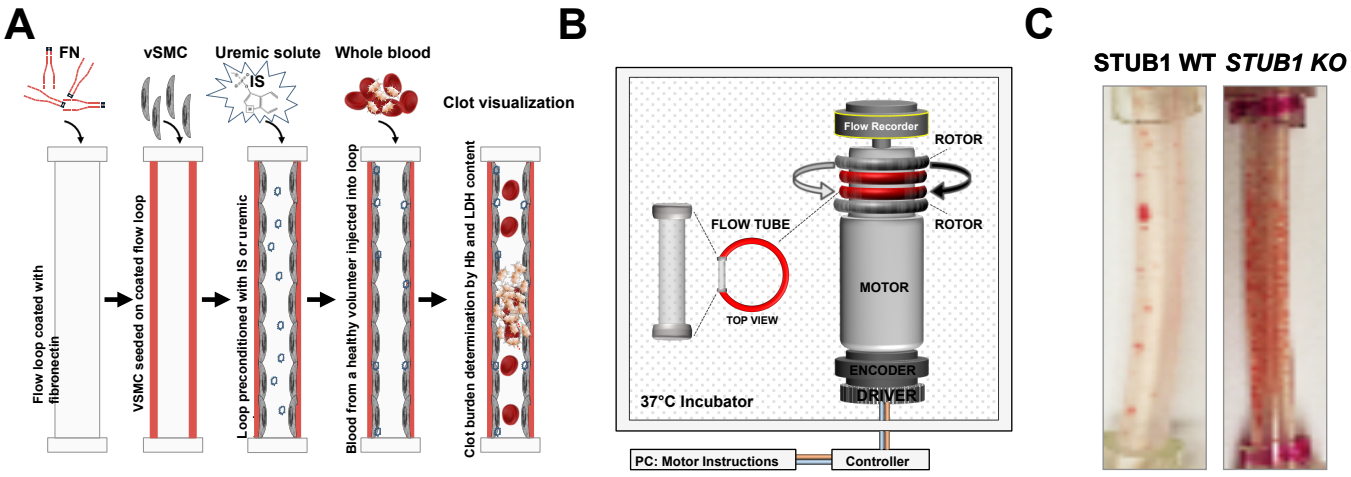
A
FN
vSMC
Uremic solute
IS
Whole blood
Clot visualization
Flow loop coated with fibronectin
VSMC seeded on coated flow loop
Loop preconditioned with IS or uremic
Blood from a healthy volunteer injected into loop
Clot burden determination by Hb and LDH content
B
Flow Recorder
ROTOR
ROTOR
FLOW TUBE
TOP VIEW
MOTOR
ENCODER
DRIVER
37°C Incubator
PC: Motor Instructions
Controller
C
STUB1 WT
STUB1 KO

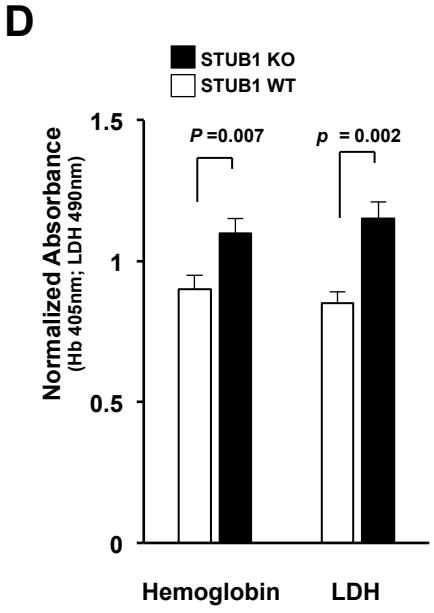
D
STUB1 KO
STUB1 WT
P =0.007
p = 0.002
Normalized Absorbance
(Hb 405nm; LDH 490nm)
1.5
1
0.5
0
Hemoglobin
LDH

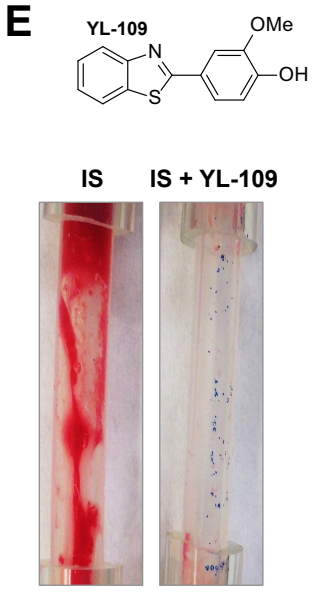
E
YL-109
OMe
OH
N
S
IS
IS + YL-109

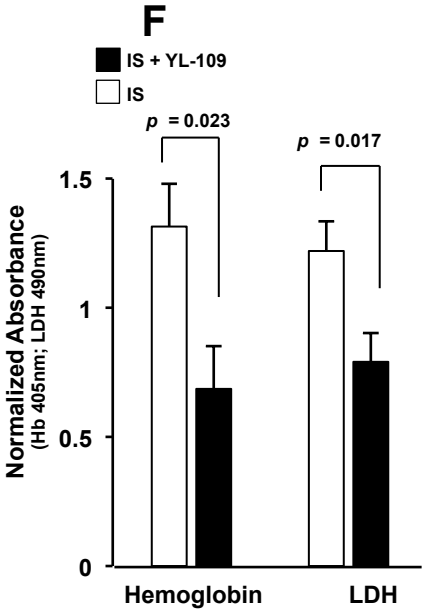
F
IS + YL-109
IS
p = 0.023
p = 0.017
Normalized Absorbance
(Hb 405nm; LDH 490nm)
1.5
1
0.5
0
Hemoglobin
LDH

Figure 4

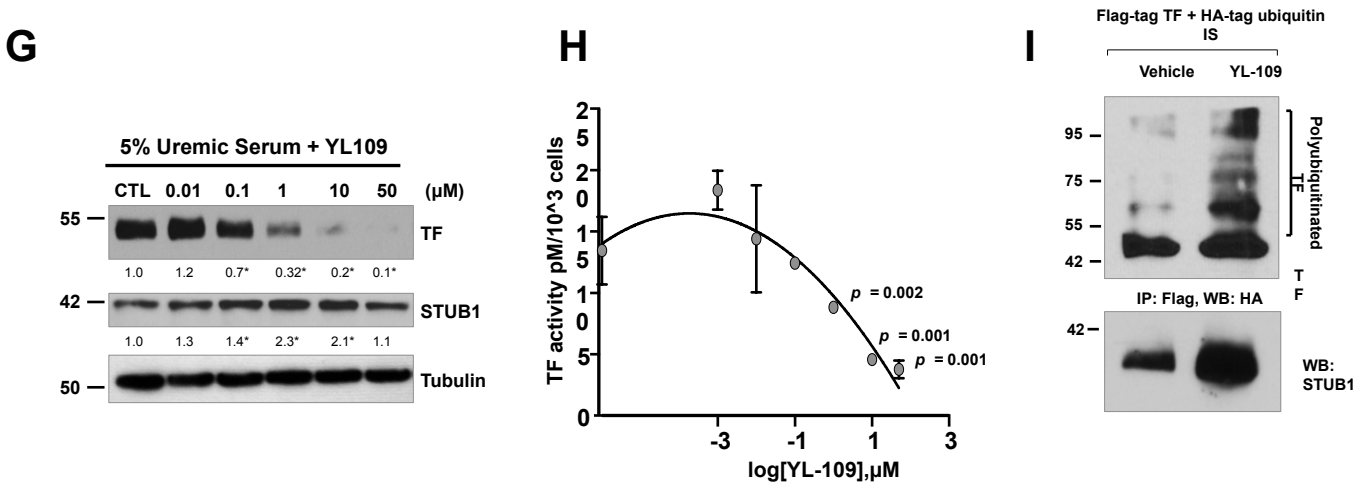
G
5% Uremic Serum + YL109
CTL 0.01 0.1 1 10 50 (μM)
55
TF
1.0 1.2 0.7* 0.32* 0.2* 0.1*
42
STUB1
1.0 1.3 1.4* 2.3* 2.1* 1.1
50
Tubulin
H
TF activity pM/10^3 cells
25
20
15
10
5
0
-3 -1 1 3
log[YL-109],μM
p = 0.002
p = 0.001
p = 0.001
I
Flag-tag TF + HA-tag ubiquitin
IS
Vehicle YL-109
95
75
55
42
Polyubiquitinated TF
TF
IP: Flag, WB: HA
42
WB: STUB1

Figure 5

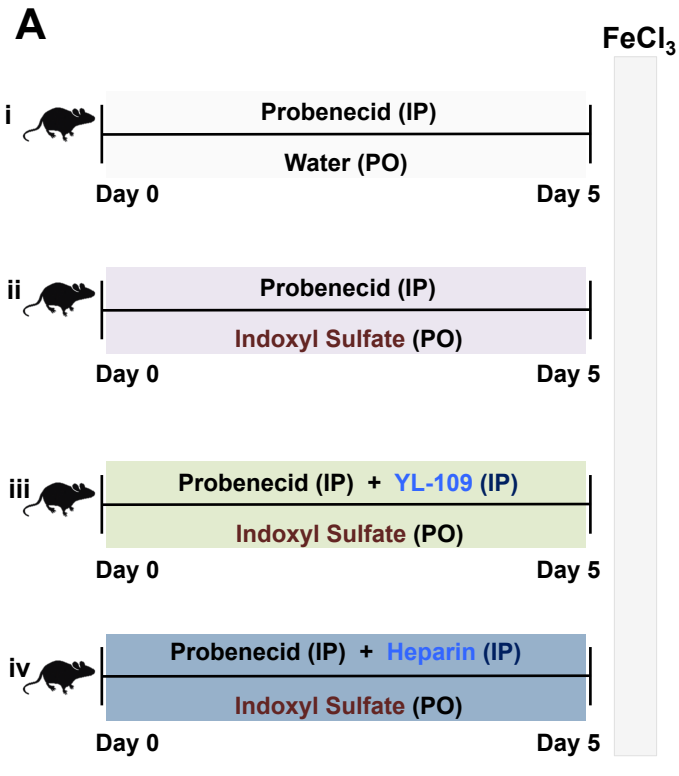
A
FeCl3
i
Probenecid (IP)
Water (PO)
Day 0
Day 5
ii
Probenecid (IP)
Indoxyl Sulfate (PO)
Day 0
Day 5
iii
Probenecid (IP) + YL-109 (IP)
Indoxyl Sulfate (PO)
Day 0
Day 5
iv
Probenecid (IP) + Heparin (IP)
Indoxyl Sulfate (PO)
Day 0
Day 5

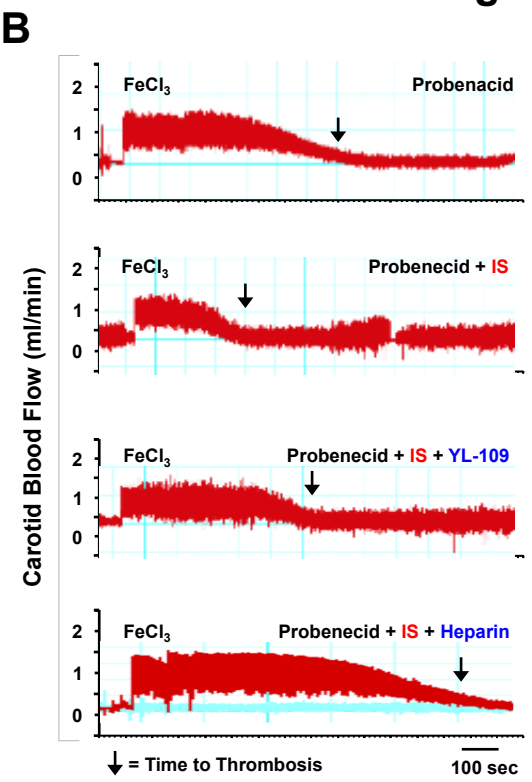
B
Carotid Blood Flow (ml/min)
FeCl3
Probenacid
Probenecid + IS
Probenecid + IS + YL-109
Probenecid + IS + Heparin
= Time to Thrombosis
100 sec

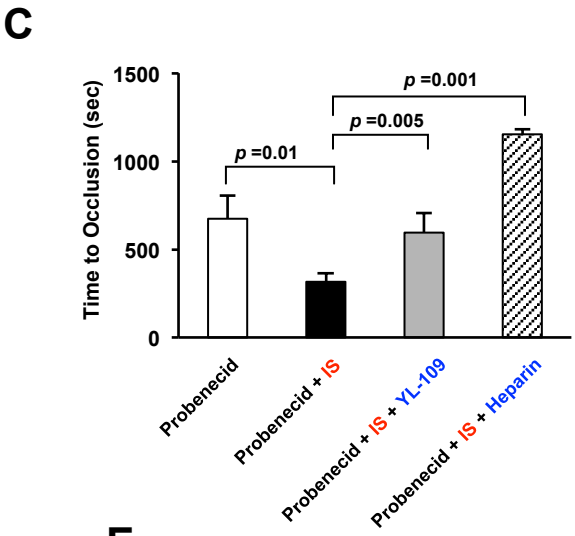
C
Time to Occlusion (sec)
p =0.01
p =0.005
p =0.001
Probenecid
Probenecid + IS
Probenecid + IS + YL-109
Probenecid + IS + Heparin

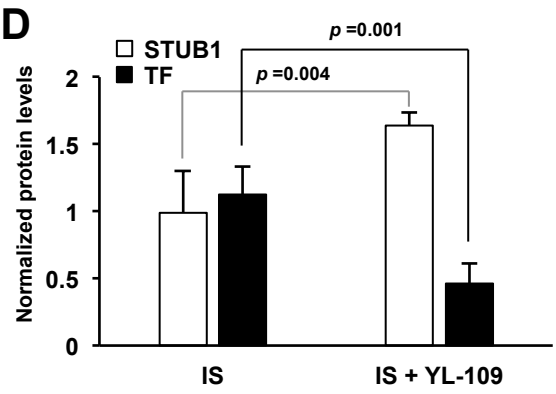
D
STUB1
TF
p =0.001
p =0.004
Normalized protein levels
IS
IS + YL-109

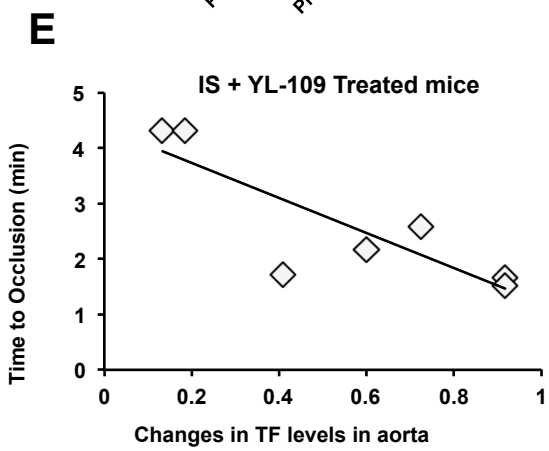
E
IS + YL-109 Treated mice
Time to Occlusion (min)
Changes in TF levels in aorta

Figure 5

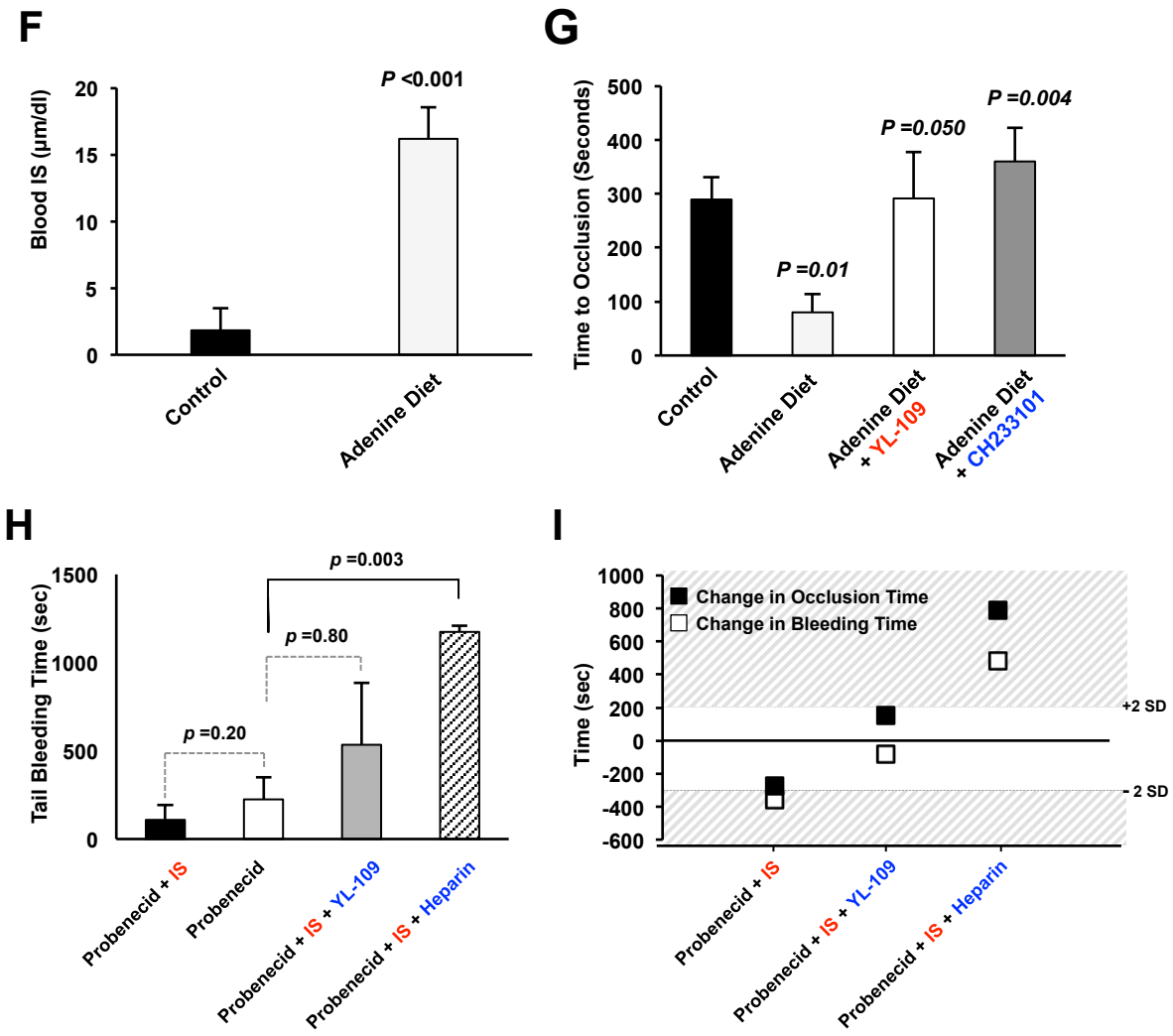
F
Blood IS (μm/dl)
20
15
10
5
0
P <0.001
Control
Adenine Diet
G
Time to Occlusion (Seconds)
500
400
300
200
100
0
P =0.01
P =0.050
P =0.004
Control
Adenine Diet
Adenine Diet + YL-109
Adenine Diet + CH233101
H
Tail Bleeding Time (sec)
1500
1000
500
0
p =0.003
p =0.80
p =0.20
Probenecid + IS
Probenecid
Probenecid + IS + YL-109
Probenecid + IS + Heparin
I
Time (sec)
1000
800
600
400
200
0
-200
-400
-600
Change in Occlusion Time
Change in Bleeding Time
+2 SD
- 2 SD
Probenecid + IS
Probenecid + IS + YL-109
Probenecid + IS + Heparin